Chapter 3

High-Resolution Respirometry: OXPHOS Protocols for Human Cells and Permeabilized Fibers from Small Biopsies of Human Muscle

Dominik Pesta and Erich Gnaiger

Abstract

Protocols for high-resolution respirometry (HRR) of intact cells, permeabilized cells, and permeabilized muscle fibers offer sensitive diagnostic tests of integrated mitochondrial function using standard cell culture techniques and small needle biopsies of muscle. Multiple substrate–uncoupler–inhibitor titration (SUIT) protocols for analysis of oxidative phosphorylation improve our understanding of mitochondrial respiratory control and the pathophysiology of mitochondrial diseases. Respiratory states are defined in functional terms to account for the network of metabolic interactions in complex SUIT protocols with stepwise modulation of coupling and substrate control. A regulated degree of *intrinsic uncoupling* is a hallmark of oxidative phosphorylation, whereas pathological and toxicological *dyscoupling* is evaluated as a mitochondrial defect. The *noncoupled* state of maximum respiration is experimentally induced by titration of established uncouplers (FCCP, DNP) to collapse the proton gradient across the mitochondrial inner membrane and measure the capacity of the electron transfer system (ETS, open-circuit operation of respiration). Intrinsic uncoupling and dyscoupling are evaluated as the flux control ratio between nonphosphorylating LEAK respiration (electron flow coupled to proton pumping to compensate for proton leaks) and ETS capacity. If OXPHOS capacity (maximally ADP-stimulated oxygen flux) is less than ETS capacity, the phosphorylation system contributes to flux control. Physiological Complex I + II substrate combinations are required to reconstitute TCA cycle function. This supports maximum ETS and OXPHOS capacities, due to the additive effect of multiple electron supply pathways converging at the Q-junction. Substrate control with electron entry separately through Complex I (pyruvate + malate or glutamate + malate) or Complex II (succinate + rotenone) restricts ETS capacity and artificially enhances flux control upstream of the Q-cycle, providing diagnostic information on specific branches of the ETS. Oxygen levels are maintained above air saturation in protocols with permeabilized muscle fibers to avoid experimental oxygen limitation of respiration. Standardized two-point calibration of the polarographic oxygen sensor (static sensor calibration), calibration of the sensor response time (dynamic sensor calibration), and evaluation of instrumental background oxygen flux (systemic flux compensation) provide the unique experimental basis for high accuracy of quantitative results and quality control in HRR.

Key words: Substrate–uncoupler–inhibitor titration, Human vastus lateralis, Needle biopsy, HEK, HPMC, HUVEC, Fibroblasts, Routine respiration, Oxidative phosphorylation, Q-junction, Pyruvate, Glutamate, Malate, Succinate, Leak, Coupling control, Uncoupling, Oxygraph, Oxygen flux, Residual oxygen consumption, Instrumental background

Carlos M. Palmeira and António J. Moreno (eds.), *Mitochondrial Bioenergetics: Methods and Protocols*, Methods in Molecular Biology, vol. 810, DOI 10.1007/978-1-61779-382-0_3, © Springer Science+Business Media, LLC 2012

Abbreviations

CCP	Coupling control protocol
E	Electron transfer system capacity
FCR	Flux control ratio
HRR	High-resolution respirometry
L	LEAK respiration
mt	Mitochondrial
O2k	Oxygraph-2k
P	OXPHOS capacity
POS	Polarographic oxygen sensor
R	ROUTINE respiration
ROX	Residual oxygen consumption
SUIT	Substrate–uncoupler–inhibitor titration
W_w	Wet weight

1. Introduction

Mitochondrial respiration is a key element of cell physiology. Cell respiration channels metabolic fuels into the bioenergetic machinery of oxidative phosphorylation, regulating and being regulated by molecular redox states, ion gradients, mitochondrial membrane potential, the phosphorylation state of the ATP system, and heat dissipation in response to intrinsic and extrinsic energy demands. Complementary to anaerobic energy conversion, mitochondrial respiration is the aerobic flux of life. It integrates and transmits a wide range of physiological and pathological signals within the dynamic communication network of the cell. This provides the background for an interdisciplinary interest in the study of mitochondrial respiratory function in biology and medicine (see Note 1).

Respirometry reflects the function of mitochondria as structurally intact organelles. It provides a dynamic measurement of metabolic flux (rates), in contrast to static determination (states) of molecular components, such as metabolite and enzyme levels, redox states and membrane potential, concentrations of signaling molecules, or RNA and DNA levels. Mitochondrial respiratory function, therefore, cannot be measured on frozen tissue samples, but usually requires minimum storage times of biological samples and delicate handling procedures to preserve structure and function. Moreover, mitochondrial respiration yields an integrative measure of the dynamics of complex coupled metabolic pathways, in contrast to monitoring activities of isolated enzymes. Measurement of respiratory flux in different metabolic states is required for evaluation of the effect on oxidative phosphorylation of changes in metabolite levels, membrane permeability, or activity of individual enzymes. Small imbalances in metabolic flux can result in large cumulative

changes of state of a metabolic system. Vice versa, even a large defect of individual enzymes may result in minor changes of flux, due to threshold effects. Hence high-quantitative resolution of respirometry is required for diagnostic applications, particularly when amounts of cells or tissue are limiting. Understanding mitochondrial respiratory control, in turn, requires experimental modulation of metabolite levels, electrochemical potentials, and enzyme activities. HRR has been developed to meet these demands and to provide the instrumental basis for modular extension with additional electrochemical and optical sensors for investigations of mitochondrial respiratory physiology (1–3).

This chapter describes applications of HRR with intact and permeabilized cells, and permeabilized muscle fibers for functional mitochondrial diagnosis. Protocols are presented for cell membrane permeabilization, biopsy sampling, short-term storage, fiber preparation, and respirometric titration regimes. The protocols provide diagnostic tests for evaluation of membrane integrity (coupling of oxidative phosphorylation; cytochrome *c* release), respiratory inhibition resulting from defects in the phosphorylation system or ETS, including respiratory complexes and activities of dehydrogenases and metabolite transporters across the inner mitochondrial membrane (4). Quality control in HRR includes traceability of basic sensor calibration, systemic flux compensation, kinetic evaluation of ADP saturation, and oxygen dependence of respiration with permeabilized fibers (2, 5), and integrates the general features of the OROBOROS Oxygraph-2k.

2. Materials

2.1. Materials for Preparation of Permeabilized Muscle Fibers

1. Nonmagnetic forceps are used for fiber preparation, one pair with sharp straight tips; one pair with sharp rounded tips; two pairs with very sharp angular tips.
2. Microbalance with five digits; 0.01 mg (Mettler-Toledo XS105DU or XS205DU) for the measurement of wet weight of fibers.

2.2. Media and Chemicals

1. Mitochondrial respiration medium (MiR05), 110 mM sucrose, 60 mM K^+-lactobionate, 0.5 mM EGTA, 3 mM $MgCl_2$, 20 mM taurine, 10 mM KH_2PO_4, 20 mM HEPES adjusted to pH 7.1 with KOH at 37 °C; and 1 g/l BSA essentially fatty acid free (6). MiR06 is MiR05 plus 280 U/ml catalase (7).
2. Relaxing and biopsy preservation solution for muscle fibers (BIOPS), 50 mM K^+-MES, 20 mM taurine, 0.5 mM dithiothreitol, 6.56 mM $MgCl_2$, 5.77 mM ATP, 15 mM phosphocreatine, 20 mM imidazole, pH 7.1, adjusted with 5 N KOH at 0 °C,

10 mM Ca–EGTA buffer (2.77 mM CaK_2EGTA + 7.23 mM K_2EGTA; 0.1 μM free calcium; ref. 8). ATP is hydrolyzed at least partially during fiber storage, thus generating millimolar levels of inorganic phosphate. It has not been tested if addition of 3 mM phosphate (9) exerts any effect on preservation quality. BIOPS can be stored at −20 °C.

3. Selected substrates, uncouplers, and inhibitors are listed in Table 1, with corresponding Hamilton syringes used for manual titrations into a 2-ml Oxygraph chamber. The sources of chemicals change according to availability and evaluation of quality and price. Information is summarized and can be updated on http://www.bioblast.at.

2.3. The Oxygraph-2k for HRR

New methodological standards have been set by HRR with the OROBOROS Oxygraph-2k (O2k; Fig. 1; OROBOROS INSTRUMENTS, Austria; http://www.oroboros.at; refs. 1–3, 10). The principle of closed-chamber HRR is based on monitoring oxygen concentration, c_{O_2}, in the incubation medium over time, and plotting oxygen consumption by the biological sample (J_{O_2}) and c_{O_2} continuously while performing the various titrations in a respirometric protocol (Figs. 2 and 5–8).

Without compromise on HRR features, the O2k provides robustness and reliability of routine instrumental performance. To increase throughput particularly in research with cell cultures and biopsy samples, the user-friendly integrated concept with full software support (DatLab) makes it possible to apply several instruments in parallel, each O2k with two independent chambers (Fig. 1). Chambers, sensors, and the electronics are shielded by a copper block and stainless steel housing. Angular insertion of the oxygen sensor into the cylindrical glass chamber places the polarographic oxygen sensor into an optimum position for stirring (Fig. 1, inset). Integrated electronic control includes Peltier temperature regulation (2–45 °C, stability ±0.001 °C), stirrer control, an electronic barometric pressure transducer for air calibration, and the optional automatic titration-injection micropump TIP2k (Fig. 1).

3. Methods

3.1. Respirometry with Intact Cells: Coupling Control Protocol

Aerobic and anaerobic metabolism is physiologically controlled in the ROUTINE state of cell respiration. Different coupling control states (4) are induced by the application of membrane-permeable inhibitors and uncouplers in a coupling control protocol (CCP; Table 2). 0.3–1.0 million fibroblasts or endothelial cells per experiment are sufficient using the OROBOROS Oxygraph-2k at 37 °C (1–3). Cell densities are adjusted to obtain maximum fluxes in the

Table 1
Selected substrates, uncouplers, and inhibitors used in SUIT protocols with isolated mitochondria or permeabilized fibers, with abbreviations (Abbr.), and site of action (electron entry, substrate entry, or inhibition of ATP synthase, CV; adenine nucleotide translocase, ANT) (37)

Substrates	Abbr.	Site of action	Concentration in syringe (solvent)	Storage (°C)	Final concentration in 2-ml O2k-chamber	Titration (µl) into 2 ml	Syringe (µl)
Pyruvate	P	CI	2 M (H_2O)	Fresh	5 mM	5	25
Malate	M	CI	0.8 M (H_2O)	–20	2 mM	5	25
Glutamate	G	CI	2 M (H_2O)	–20	10 mM	10	25
Succinate	S	CII	1 M (H_2O)	–20	10 mM	20	50
Octanoylcarnitine	Oct	ETF	0.1 M (H_2O)	–20	0.2 mM	4	10
Ascorbate	As	CIV	0.8 M (H_2O)	–20	2 mM	5	25
TMPD[a]	Tm	CIV	0.2 M (H_2O)	–20	0.5 mM	5	25
Cyt.	c	CIV	4 mM (H_2O)	–20	10 µM	5	25
ADP	D	CV, ANT	0.5 M (H_2O)	–80	1–5 mM	4–20	10
ATP	T	CV, ANT	0.5 M (H_2O)	–80	1–5 mM	4–20	10
Uncoupler							
FCCP[b]	F	$\Delta\mu_{H+}$	1 mM (EtOH)	–20	0.5 µM steps	1 µl steps	10
FCCP	F	$\Delta\mu_{H+}$	0.1 mM (EtOH)	–20	0.05 µM steps	1 µl steps	10
Inhibitors							
Rotenone	Rot	CI	1.0 mM (EtOH)	–20	0.5 µM	1	10
Malonic acid	Mna	CII	2 M (H_2O)	Fresh	5.0 mM	5	25
Antimycin A	Ama	CIII	5 mM (EtOH)	–20	2.5 µM		10

(continued)

Table 1
(continued)

Substrates	Abbr.	Site of action	Concentration in syringe (solvent)	Storage (°C)	Final concentration in 2-ml O2k-chamber	Titration (µl) into 2 ml	Syringe (µl)
Myxothiazol	Myx	CIII	1 mM (EtOH)	–20	0.5 µM	1	10
Sodium azide	Azd	CIV	4 M (H_2O)	–20	≥100 mM	≥50	50
KCN	Kcn	CIV	1 M (H_2O)	Fresh	1.0 mM	2	10
Oligomycin	Omy	CV	4 mg/ml (EtOH)	–20	2 µg/ml	1	10
Atractyloside	Atr	ANT	50 mM (H_2O)	–20	0.75 mM	30	50

[a] *N*,*N*,*N*,*N*′,*N*′-tetramethyl-*p*-phenylenediamine dihydrochloride
[b] Carbonyl cyanide *p*-trifluoromethoxyphenylhydrazone

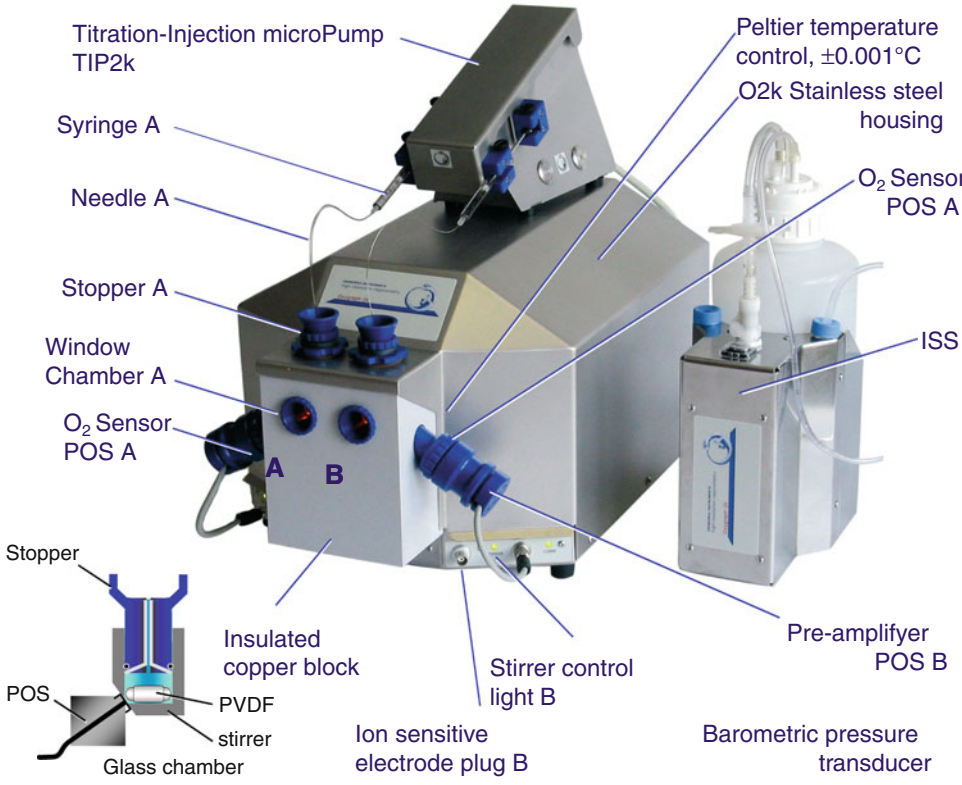

Fig. 1. Oxygraph-2k for high-resolution respirometry (O2k Series C) with TIP2k and integrated suction system (ISS). Two glass chambers (A and B) are housed in an insulated copper block with electronic Peltier temperature control. Polarographic oxygen sensors (POS) are sealed by a butyl rubber gasket against the angular plane on the glass chambers. The PVDF (or PEEK) stirrers are powered by electrically pulsed magnets inserted in the copper block. Stoppers contain a capillary for extrusion of gas bubbles and insertion of a needle for manual or automatic titrations with the TIP2k. Additional capillaries through the stopper (PVDF) are drilled for insertion of various electrodes, the signals of which are simultaneously recorded by the DatLab software. Copyright ©2010 by OROBOROS INSTRUMENTS. Reproduced with permission; http://www.oroboros.at.

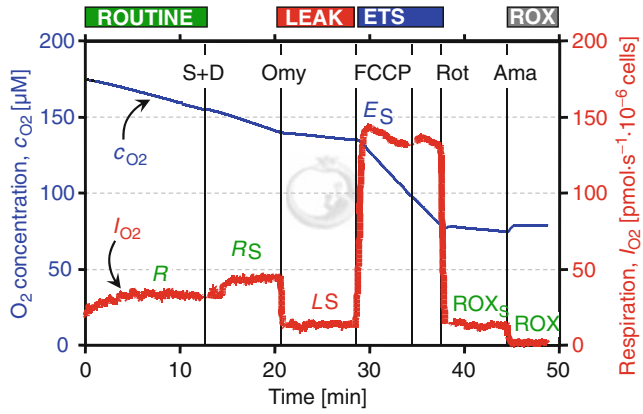

Fig. 2. Coupling control protocol and respirometric cell viability test, showing continuous traces of respiration of human peritoneal mesothelial cells [I_{O_2} (pmol/s per 10^6 cells)], calculated as the negative time derivative of oxygen concentration, c_{O_2} . 0.5×10^6 cells/ml in MiR05 (80% viability; 2-ml chamber, 37 °C). Endogenous ROUTINE respiration without substrates (*R*), addition of 10 mM succinate and 5 mM ADP (S + D), 1 µg/ml oligomycin (Omy; LEAK state, *L*), stepwise 1 µM titration of FCCP (ETS capacity, state *E*), and inhibition by 0.5 µM rotenone (Rot) and 2.5 µM antimycin A (Ama) for the final measurement of residual oxygen consumption (ROX). Oxygen flow is not shown immediately after titrations, when oxygen concentration and the calculation of slopes are disturbed particularly when ethanol is the solvent. Modified after ref. 19.

Table 2
Electron transfer system (ETS) capacity and flux control ratios (FCRs)[a] in the coupling control protocol with intact human (and 32D mouse) cells (37 °C; mean ± SD)

Cell type	ETS, *E* (pmol/s/10^6)	*ROUTINE, R/E*	*LEAK, L/E*	*netROUTINE, (R – L)/E*	Residual, ROX/*E′*	References
HEK 293[b]	14 ± 2	0.31 ± 0.03	0.09 ± 0.00	0.23 ± 0.02	0.01 ± 0.00	(17)
32D (mouse)[c]	81 ± 11	0.39 ± 0.02	0.10 ± 0.02	0.29 ± 0.02	0.03 ± 0.01	(3)
CEM – Control[d]	54 ± 11	0.40 ± 0.03	n.d.	n.d.	0.02 ± 0.03	(12)
CEM – G1-phase, apopt.[d]	31 ± 6	0.41 ± 0.03	n.d.	n.d.	0.03 ± 0.03	(12)
CEM – S-phase, apopt.[d]	85 ± 13	0.38 ± 0.03	n.d.	n.d.	0.01 ± 0.01	(12)
HUVEC[e]	114 ± 18	0.26 ± 0.02	0.13 ± 0.02	0.13 ± 0.00	0.05 ± 0.04	(16)
HPMC Control[f]	181 ± 58	0.40 ± 0.09	0.09 ± 0.01	0.31 ± 0.08	0.005 ± 0.01	(19)
HPMC + IL-1β[f]	142 ± 47	0.41 ± 0.09	0.08 ± 0.02	0.32 ± 0.08	0.02 ± 0.01	(19)
Fibroblasts – Young[g]	111 ± 24	0.34 ± 0.03	0.14 ± 0.02	0.20 ± 0.02	0.07 ± 0.03	(15)
Fibroblasts – Young arrest[g]	138 ± 22	0.23 ± 0.01	0.05 ± 0.01	0.18 ± 0.02	0.05 ± 0.00	(15)
Fibroblasts – Senescent[g]	285 ± 72	0.42 ± 0.05	0.21 ± 0.04	0.21 ± 0.05	0.07 ± 0.03	(15)

[a]Capacity of the ETS (pmol/s per 10^6 cells) is the reference for normalization of *FCR*, $E = E' - \mathrm{ROX}$, where E' is the apparent (uncorrected) electron transfer capacity. Similarly, $R = R' - \mathrm{ROX}$ and $L = L' - \mathrm{ROX}$. To calculate total ROUTINE respiration (R' (pmol/s per 10^6 cells)) $R' = \left((R/E) + (\mathrm{ROX}/E') / (1 - \mathrm{ROX}/E')\right) \times E$

[b]Transformed human embryonic kidney cells (10×10^6/ml); $N = 3$–8 independent cell cultures in culture medium DMEM

[c]Mouse parental hematopoietic cells (1.1×10^6/ml); $n = 6$, replicate O2k measurements of a single suspension culture in culture medium RPMI

[d]Human leukemia cells (1.0×10^6/ml to 1.2×10^6/ml); controls ($N = 27$), and 30% apoptotic cultures preincubated with dexamethasone, arrested in the G1-phase ($N = 9$) or with gemcitabine, arrested in the S-phase ($N = 12$) in culture medium RPMI; n.d., not determined

[e]Human umbilical vein endothelial cells (0.9×10^6/ml); $N = 3$; in culture medium EGM

[f]Human peritoneal mesothelial cells (0.6×10^6/ml); $N = 5$; cultured from five donors, incubated for 48 h without (controls) or with recombinant IL-1β. ROUTINE respiration in MiR05 with succinate and ADP (Fig. 2)

[g]Human foreskin fibroblasts; young ($n = 12$; 1.0×10^6/ml), young-cell cycle arrest ($n = 5$; 1.1×10^6/ml), and senescent ($n = 12$; 0.2×10^6/ml), in culture medium DMEM

range of 30–300 pmol/s ml. It takes 50–90 min for the evaluation of mitochondrial coupling states (Fig. 2).

Respiratory flow, I_{O_2}, of intact cells is expressed per million viable cells (Table 2). Cell viability should be >0.95 in the control group of various cell types (HUVEC, fibroblasts). Mass-specific oxygen flux, J_{O_2}, is expressed per mg dry weight (11) or cell protein (12). Mitochondrial (mt) marker-specific respiration is obtained by normalization of flux relative to a mt-marker, such as citrate synthase (CS) or cytochrome *c* oxidase activity (12). Internal normalization yields flux control ratios relative to flux in a common reference state (Table 2).

3.1.1. ROUTINE Respiration

Cellular ROUTINE respiration (*R*) and growth is supported by exogenous substrates in culture media (3, 11–17). In media without energy substrates, respiration is based on endogenous substrates. Physiological energy demand, energy turnover, and the degree of coupling (intrinsic uncoupling and pathological dyscoupling) control the levels of respiration and phosphorylation in the physiological coupling state *R* of intact cells. The maximum capacity of oxidative phosphorylation (OXPHOS; analogous to State 3; ref. 18) cannot be studied by external addition of ADP to intact cells, since the plasma membrane is impermeable to ADP and many mitochondrial substrates (11–14, 19). However, evaluation of the Crabtree effect upon addition of glucose (20) is possible only in intact cells. *R* in human cells (Table 2) ranges from 4 pmol/s per 10^6 cells in the small HEK cells (17), 30–40 pmol/s per 10^6 (HUVEC and fibroblasts; ref. 11, 15), and 70 pmol/s per 10^6 (mesothelial cells; ref. 19), compared to 250 pmol/s per 10^6 for the much larger rat hepatocytes (21).

3.1.2. LEAK State

Following stabilization of *R*, ATP synthesis is inhibited by oligomycin (atractyloside or carboxyatractyloside; Table 1). In this nonphosphorylating or resting LEAK state (*L*; analogous to State 4; ref. 18), LEAK respiration reflects intrinsic uncoupling as (i) compensation for the proton leak at maximum mitochondrial membrane potential, (ii) proton slip (decoupled respiration), (iii) electron slip which diverts electrons toward reactive oxygen species (ROS) production, and (iv) cation cycling (Ca^{2+}, K^+) (3, 4). Monitoring *L* should be limited to <5 min (Fig. 2), to avoid secondary effects on coupling and respiratory capacity.

3.1.3. ETS Capacity

Mitochondrial respiratory control by the phosphorylation system is partially or fully released by pathophysiological uncoupling and dyscoupling, or experimentally by titration of a protonophore such as FCCP (Table 1). In the noncoupled, open proton circuit, the electrochemical proton potential across the inner mitochondrial membrane is collapsed. Uncoupler titration, therefore, removes

the electrochemical backpressure on the proton pumps (Complexes CI, CIII, and CIV) and stimulates respiration maximally at level flow as a measure of ETS capacity in the noncoupled state *E* (Fig. 2). It is important to titrate an optimum concentration of uncoupler, beyond which respiration is inhibited (3, 11). Optimum uncoupler concentrations depend on cell type, cell concentration, medium, and permeabilized versus intact cells. Inhibition of *E* by oligomycin should be evaluated by uncoupler titrations in the absence of inhibitor. *E* ranges from 14 to 180 pmol/s per 10^6 cells in HEK, CEM, HUVEC, fibroblasts, and mesothelial cells, largely depending on cell size. ETS capacity per cell doubles with cell size in CEM cells after cell cycle arrest in the G_1- versus S-phase, and in senescent fibroblasts (Table 2).

3.1.4. Residual Oxygen Consumption

Residual oxygen consumption (ROX) remains after inhibition of the ETS. Mitochondrial respiratory states *R*, *L*, and *E* are corrected for ROX (Table 2). Many cellular oxygen consuming enzymes and autooxidation reactions give rise to ROX, including peroxidase and oxidase activities which partially contribute to ROS production. It is difficult to evaluate exactly the extent to which inhibitors of the ETS (Table 1) exert an influence on ROX. Cyanide and azide inhibit CIV and other heme-containing enzymes such as catalase, and may thus modify ROX. Valuable information on ROX is obtained by sequential titration of inhibitors (Fig. 2). Rotenone inhibits cell respiration of human fibroblasts and HUVEC, without a further decline of ROX after the addition of antimycin A (15, 16).

3.1.5. Coupling Control Ratios from the Coupling Control Protocol

Flux control ratios (FCRs) express respiratory control independent of mitochondrial content and cell size. FCRs are normalized for maximum flux in a common reference state, to obtain theoretical lower and upper limits of 0.0 and 1.0 (0 and 100%; Table 2).

1. ROX/*E*′: The ROX/*E*′ ratio is low (0.01–0.07; Table 2), but ROX contributes to a significant extent to LEAK respiration, with corresponding ROX/*L*′ ratios ranging from 0.1 to 0.3, and up to 0.5 in growth-arrested fibroblasts (Table 2).
2. *L*/*E*: The LEAK control ratio is the ratio of LEAK respiration and ETS capacity. *L*/*E* ranges from 0.09 to 0.14 in various cells (Table 2; the inverse, 11–7, is the respiratory control ratio, RCR; ref. 4, 18). Dyscoupling increases the *L*/*E* ratio, e.g., to 0.21 in senescent fibroblasts (Table 2). Alternatively, the *L*/*E* ratio may increase without intrinsic uncoupling or dyscoupling, if ETS capacity is diminished. It is, therefore, important to evaluate potential defects of ETS capacity per mt-marker, e.g., ETS per citrate synthase activity (12, 15, 19).
3. *R*/*E*: The ROUTINE control ratio is the ratio of (coupled) ROUTINE respiration and (noncoupled) ETS capacity.

R/E ranges from 0.2 to 0.4 (Table 2; the inverse of 5–2.5 is the uncoupling control ratio, UCR; ref. 3, 11–15). The R/E ratio is an expression of how close ROUTINE respiration operates to ETS capacity. Reported R/E ratios ≥0.5 (22) could not be reproduced by HRR in a wide range of human cell types and incubation conditions (Table 2). The discrepancies cannot be fully explained by high glucose concentrations in culture and respiration media, since glucose exerts an effect not only on R but also on E (20). R/E ratios increase due to (i) high ATP demand and ADP-stimulated ROUTINE respiration, (ii) dyscoupling (senescent fibroblasts; Table 2), and (iii) limitation of respiratory capacity by the defects of substrate oxidation and complexes of the ETS.

4. $(R-L)/E$: The netROUTINE control ratio, $(R-L)/E$, expresses phosphorylation-related respiration (corrected for LEAK respiration) as a fraction of ETS capacity. 0.1–0.3 of *ETS* capacity is used for oxidative phosphorylation under ROUTINE conditions (Table 2). $(R-L)/E$ remains constant, if dyscoupling is fully compensated by an increase of ROUTINE respiration and a constant rate of oxidative phosphorylation is maintained (fibroblasts in Table 2). Upon stimulation of ROUTINE respiration by an increased ATP demand or if the ETS capacity declines without effect on R, however, $(R-L)/E$ increases, which indicates that a higher proportion of the maximum capacity is activated to drive ATP synthesis. $(R-L)/E$ declines to zero in either fully uncoupled cells ($R=L=E$) or in cells under metabolic arrest ($R=L<E$).
5. If the PC protocol is extended by the measurement of cytochrome *c* oxidase, then the ratio of CIV activity and noncoupled respiration is an index of the apparent excess capacity of this enzyme step in the ETS. Autooxidation of ascorbate and TMPD (Table 1) is extremely high in culture media, hence a mitochondrial respiration medium is used (12).

3.1.6. Respirometric Viability Index

Two quantitative indices of cell membrane permeability (cell viability) are derived from the protocol shown in Fig. 2 (19, 23). (i) The stimulatory effect of succinate + ADP is related to cell membrane permeabilization as $(R_S-R)/(E_S-R)$. The permeable cells are depleted of substrates and adenylates, hence succinate + ADP stimulates respiration, $R_S-R>0$, in permeabilized cells only. (ii) Stepwise inhibition by rotenone (CI) and antimycin A (CIII) is related to cell membrane permeabilization as $(ROX_S-ROX)/E_S$. $E_S=E_S'-ROX$ is the ETS capacity. CII respiration is inactivated in intact cells after inhibition of CI by rotenone, since external succinate cannot penetrate the plasma membrane, succinate production

by the tricarboxylic acid cycle (TCA) is stopped when NADH cannot be oxidized, and there are no cytosolic sources of succinate. Addition of succinate to intact cells, therefore, does not exert any effect on respiration, $ROX_S - ROX = 0$ (11, 13). $ROX_S - ROX$ represents succinate-supported respiration of permeable cells (in the presence of the CI inhibitor rotenone, Rot) over antimycin A-inhibited ROX of all cells.

These respiratory viability indices are based on preserved respiratory function in mt-respiration medium after cell membrane injury, whereas respiration of permeabilized cells is fully inhibited by high Ca^{2+} in culture media (23, 24). The respirometric approach was confirmed by agreement between respirometric viability (0.79 ± 0.03 and 0.80 ± 0.03 for controls and IL-1β exposed cells) and cell viability (0.87 ± 0.03 and 0.79 ± 0.02; mean ± SD) obtained with a CASY 1 Cell Counter and Analyser System (Schaerfe System, Germany; ref. 19).

3.2. Preparation of Permeabilized Cells and Muscle Fibers

Extended functional OXPHOS analysis requires isolation of mitochondria or controlled plasma membrane permeabilization, with effective wash-out of free cytosolic molecules including adenylates, substrates, and cytosolic enzymes, making externally added compounds accessible to the mitochondria (14, 25–29). Full mechanical permeabilization of cell membranes is achieved in liver tissue (29). Biopsy sampling and mechanical fiber preparation lead to partial permeabilization of skeletal muscle. Without homogenous cell membrane integrity, respiration cannot be studied in the ROUTINE state. At low concentrations, digitonin or saponin permeabilize the plasma membranes completely and selectively due to their high cholesterol content, whereas mitochondrial membranes with lower cholesterol content are affected only at higher concentrations. Mitochondrial isolation is more time-consuming than cell membrane permeabilization. Merely 1 or 2 mg wet weight of cardiac or skeletal muscle fibers is sufficient for individual experimental runs with the OROBOROS Oxygraph-2k, but >70 mg is required even for micropreparations of isolated mitochondria (30). The homogeneous suspension of isolated mitochondria yields a representative average for large tissue samples, whereas tissue heterogeneity contributes to the variability of results with small samples of permeabilized fibers. Mitochondria can be isolated to separate different mitochondrial subpopulations (31). Isolated mitochondria and small cultured cells are the appropriate models for the study of mitochondrial oxygen kinetics ((1, 2, 5, 10, 11, 17, 20, 32–34); see Note 2).

3.2.1. Permeabilization of Cells

1. After air calibration of the oxygen sensors in the O2k-chamber with MiR06, the medium is siphoned off.

2. Cells are suspended in respiration medium at a final cell density such that ROUTINE respiration yields a volume-specific oxygen flux of about 20 pmol/s per cm^3, or higher (Fig. 2). Up to 3 ml are added into each O2k-chamber, while rotation of the stirrers is maintained. Samples can now be collected from the stirred chambers containing a homogenous cell suspension, for the analysis of cell count, cell volume, and cell viability (CASY, Schaerfe System, Germany), protein concentration, and enzyme assays. A minimum of 2.1-ml cell suspension must remain in the chamber.
3. Close the chambers by fully inserting the stoppers into the volume-calibrated position, thereby extruding all gas bubbles. Siphon off any excess cell suspension from the receptacle of the stoppers.
4. Start data acquisition with a new file, and allow endogenous *R* to stabilize for 15–20 min (compare Fig. 2).
5. Titrate the first selected substrates into the chamber (e.g., glutamate + malate), and add digitonin at optimum concentration, e.g., 10 μg per 10^6 cells. Observe a gradual decline of respiration due to cell membrane permeabilization and loss of adenylates from the cytosol, allow *L* to stabilize, and proceed with a SUIT protocol (Subheading 3.3.4).
6. Optimum digitonin concentrations for complete plasma membrane permeabilization of cultured cells can be determined directly in a respirometric protocol (Fig. 3), which may be used simultaneously for selecting optimum experimental cell concentrations. After inhibition of endogenous *R* by rotenone, respiration of intact cells (viability >0.95) is not stimulated by the addition of succinate and ADP (compare Fig. 2, with cell viability of 0.8). Subsequent stepwise digitonin titration yields gradual permeabilization of plasma membranes, shown by the increase of respiration up to full permeabilization (Fig. 3; at 10 μg per 10^6 cells). Respiration is constant over a range of optimum digitonin concentrations, but is inhibited at higher concentrations when the outer mitochondrial membrane becomes affected and cytochrome *c* is released (cytochrome *c* test, see Subheading 3.3.2). Respiration of permeabilized cells is stable during SUITs in the presence of an optimum digitonin concentration.

3.2.2. Muscle Biopsy and Short-Term Storage

This project was approved by the Ethics Committee of the Medical University of Innsbruck (AN3433 271/4.12). In sports physiology, it is important to choose a muscle for biopsy sampling that is actively involved in the motion of interest. The human muscle most extensively studied for functional diagnosis of mitochondrial

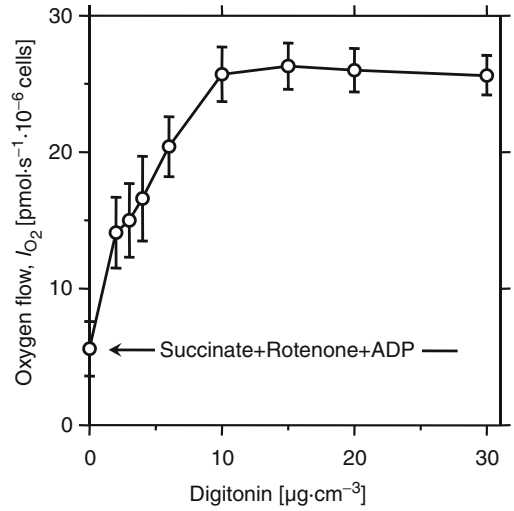

Fig. 3. Protocol for determination of optimum digitonin concentration for selective cell membrane permeabilization by respirometry and titration of digitonin to initially intact cells suspended in mitochondrial medium, in the presence of 10 mM succinate, 0.5 µM rotenone, and 1 mM ADP. Human umbilical vein endothelial cells transformed by lung carcinoma at a density of 1.02 (±0.16) × 10^6 per cm^3 (N = 6; ±SD). 12–14 min time intervals between titrations up to 3 µg/cm^3, 4–5 min at higher digitonin concentrations. Permeabilization at a digitonin concentration of 10 µg per 10^6 cells is optimum for ADP-stimulated respiration. From ref. 26.

diseases is the quadriceps (m. vastus lateralis; ref. 4) as it is easily accessible and major nerves and blood vessels lie close to the femur and are unlikely to be injured during biopsy sampling (35). Ultrasound imaging is a simple and quick technique to assess the site and depth of biopsies, can be applied before taking a biopsy, and can be performed in the outpatient clinic. If the depth is not controlled, this may affect the outcome due to differences in fiber type distribution in the muscle (35). Eight O2k-chambers were operated simultaneously for high throughput of biopsied samples.

1. When applying the local anesthetic, it is important not to infiltrate the muscle since several anesthetics exert a direct effect on mitochondrial function.
2. After taking the biopsy, the tissue is removed from the Bergstrom needle with a pair of forceps (rounded tip). The tissue is placed onto a precooled Petri dish on ice, and – if necessary – cut diagonally into small portions of 5–10 mg wet weight (W_w), using a sharp scalpel. These subsamples thus have largely equivalent fiber types.
3. Subsamples of 5 mg W_w for HRR are placed quickly into small tubes with 3–4 ml ice-cold BIOPS for two replicate measurements. In this preservation solution, the sample can be stored for several hours at 0 °C, depending on the source of muscle

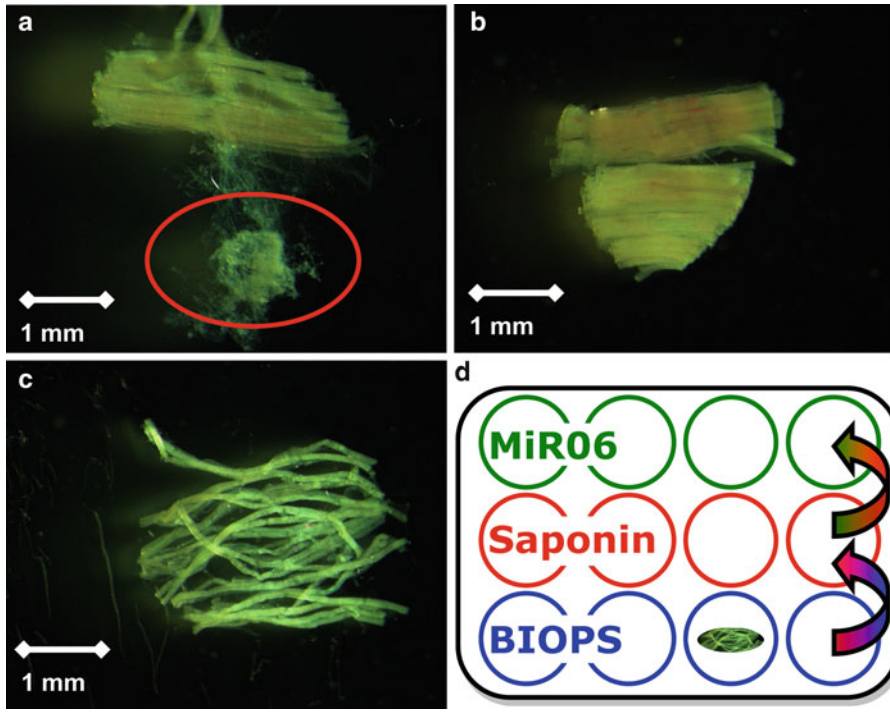

Fig. 4. Preparation of permeabilized muscle fibers from a small biopsy of human vastus lateralis. (**a**) A large amount of connective tissue (*circle*) is removed. (**b**) Muscle fiber bundle. (**c**) Fiber bundles after mechanical separation with a pair of forceps with very sharp angular tips (standardized period of 4 min). Mesh-like structure and change in color from reddish to pale due to loss of myoglobin and removal of remaining vessels. (**d**) 12-well plate (Falcon 35/3043) for permeabilization of muscle fibers for four respiratory chambers with sequential incubation in BIOPS, saponin, and MiR06.

tissue (human skeletal muscle for 24 h; ref. 9). This provides the possibility for shipping of biopsies on ice for functional analysis by HRR.

4. Subsamples for other assays (histochemical/morphological; enzymatic; mtDNA) are stored in assay-specific media or liquid nitrogen.

3.2.3. Mechanical Preparation of Permeabilized Fibers

1. The tissue sample with BIOPS solution is transferred onto a small Petri dish on an ice-cold metal plate.
2. Connective tissue is removed using two pairs of very sharp angular forceps (Fig. 4a).
3. Fiber bundles are separated mechanically with these forceps over a standardized period of 4 min for the preparation of a 2-mg sample of human v. lateralis. Fibers are partially teased apart and stretched out, remaining connected in a mesh-like framework (Fig. 4c). Proper separation and a change from red to pale color are best observed against a dark background (Fig. 4a–c). At least during a start-up period, it is recommended to use a dissecting scope for effective removal of connective tissue and observation of the mechanical separation.

Initially, difficulties arise frequently from the application of excess tissue, which makes mechanical separation tedious.

4. Fiber bundles of similar mass are placed sequentially into 2-ml ice-cold BIOPS in individual wells (Fig. 4d).

3.2.4. Chemical Permeabilization and Wet Weight of Muscle Fibers

1. After fibers for all simultaneously operated O2k-chambers are mechanically prepared and placed into the wells with ice-cold BIOPS, the fiber bundles are transferred quickly into 2 ml freshly prepared saponin solution (50 µg/ml BIOPS; add 20 µl saponin stock solution of 5 mg saponin/ml BIOPS into 2 ml BIOPS; Fig. 4d).
2. Shake by gentle agitation in the cold room (on ice) for 30 min.
3. Transfer all samples from the saponin solution into 2 ml of MiR06 (Fig. 4d). Continue shaking by gentle agitation for 10 min in the cold room (on ice).
4. Wet weight measurements are made after permeabilization, which reduces osmotic variations in water contents. Loosely connected fiber bundles (skeletal muscle 1–3 mg W_w; heart 0.5–2 mg W_w) are taken with the pair of sharp forceps (rounded tip) and placed for 5 s onto dry filter paper. During this time, wipe off any liquid from the tip of the forceps with another filter paper. Take the sample from the filter paper, touch it once more shortly onto a dry area of filter paper while holding it with the forceps, and place the sample onto a small plastic plate on the table of the tared balance.
5. Immediately after reading the W_w, the sample is transferred into a separate droplet of ice-cold MiR06 on a large Petri dish. Check that the tare balance reading returns to zero. Each droplet contains a sample for a respirometric experiment.
6. A pair of forceps with straight tips is used to fully immerse the fibers into the medium in the O2k-chamber. Check if the entire tissue sample has been removed from the droplet into the O2k-chamber.
7. Full permeabilization is validated by a decline of LDH activity to 1% of intact tissue (8), or more quickly by respirometry. Respiration of fully permeabilized tissue is not increased by titration of saponin or digitonin in the presence of substrate and ADP. A stimulatory effect of saponin, however, indicates incomplete permeabilization of muscle fibers that were not incubated in saponin solution prior to the experimental run (Fig. 5). Saponin-permeabilization in the respiration chamber does not yield maximum respiratory capacity of muscle fibers. The larger saponin-stimulation of respiration indicated a lower degree of permeabilization (Fig. 5b), which correlated with lower mass-specific oxygen flux even after addition of saponin (compare Fig. 5a).

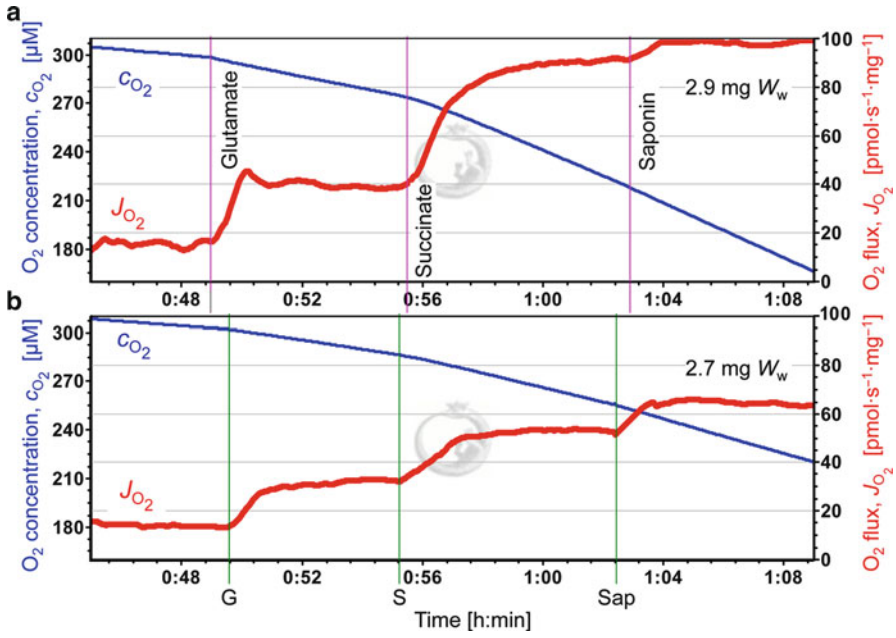

Fig. 5. Saponin test for cell membrane permeabilization. Oxygraph traces of oxygen concentration (c_{O_2}) and mass-specific oxygen flux [J_{O_2} (pmol O_2/s per mg W_w)]. Fibers of human vastus lateralis were mechanically but not chemically permeabilized before incubation. Partial permeabilization of the cell membrane is shown by the stimulatory effect of glutamate (G) and succinate (S) in the presence of malate, octanoylcarnitine, and ADP (2.5 mM), whereas lack of full permeabilization is seen by further stimulation of respiration after addition of saponin (50 µg/ml). 37 °C, MiR06, 2 ml O2k-chamber. (**a**) 2.9 mg W_w. (**b**) 2.7 mg W_w. Experiment 2010-03-08 AB-01.

3.3. HRR with Permeabilized Muscle Fibers, Permeabilized Cells, and Isolated Mitochondria

3.3.1. Temperature

The further the experimental conditions differ from the physiological reference state, the larger the error becomes which may result from adjustment to 37 °C of respiratory fluxes in various metabolic states, applying a commonly assumed constant temperature coefficient. Assuming a Q_{10} of 2 (multiplication factor for flux at a 10 °C difference), the temperature coefficients for rates measured at 22, 25, or 30 °C are 2.83, 2.30, and 1.62, respectively, to convert to respiration at 37 °C. Some fundamental functional properties of mitochondria change at 25 °C, for instance, there is a shift from proton leak at 37 °C (proton flux through the membrane) to proton slip at 25 °C (protons pulled back into the matrix phase within a proton pump; ref. 36). In mitochondrial physiology, therefore, experimental temperature close to body temperature has become a standard for quantitative evaluation of mitochondrial respiratory function in mammalian cells (Table 2) and tissues (4).

3.3.2. Substrates: Electron Donors

Mitochondrial respiration depends on a continuous flow of electron-supplying substrates across the mitochondrial membranes into the matrix space. Many substrates are strong anions that cannot permeate lipid membranes and hence require carriers. Various anion carriers in the inner mitochondrial membrane are involved in the transport of mitochondrial metabolites.

Their distribution across the mitochondrial membrane varies mainly with ΔpH and not with Δψ, since most carriers (but not the glutamate-aspartate carrier) operate nonelectrogenically by anion exchange or co-transport of protons. Depending on the concentration gradients, these carriers also allow for the transport of mitochondrial metabolites from the matrix into the cytosol and for the loss of intermediary metabolites into the incubation medium. Export of intermediates of the TCA plays an important metabolic role in the intact cell. This must be considered when interpreting the effect on respiration of specific substrates used in studies of permeabilized cells and isolated mitochondria (4, 37). Some typical saturating substrate concentrations used in respiratory studies are listed in Table 1.

1. Electron donors for NAD^+ and Complex I: Substrate combinations of pyruvate + malate (PM) and glutamate + malate (GM) activate dehydrogenases yielding reduced nicotinamide adenine dinucleotide (NADH), which feeds electrons into CI (NADH-ubiquinone oxidoreductase) and hence down the thermodynamic cascade through the Q-cycle, CIII, cytochrome *c*, CIV, and ultimately O_2. Electrons flow from NADH to oxygen with three proton pumps (CI, CIII, and CIV) in series.
2. Complex II is the only membrane-bound enzyme in the TCA cycle. The flavoprotein succinate dehydrogenase is the largest polypeptide of CII. Following succinate oxidation, the enzyme transfers electrons directly to the quinone pool (38). Whereas CI is NADH-linked *upstream* to the dehydrogenases of the TCA, CII is $FADH_2$-linked *downstream* with subsequent electron flow to the Q-junction (4, 37). Electrons flow from succinate to oxygen with two proton pumps (CIII and CIV) in series.
3. Studies of fatty acid oxidation involve a large variety of substrates, such as palmitic acid, palmitoylcarnitine, or palmitoyl-CoA with carnitine. Like CII, electron-transferring flavoprotein (ETF) is located on the matrix face of the inner mitochondrial membrane. It supplies electrons from fatty acid β-oxidation to CoQ. For β-oxidation to proceed, convergent electron flow into the Q-junction is obligatory from both CI and ETF. Malate is provided, therefore, simultaneously with fatty acid substrates, and fatty acid oxidation is blocked by inhibition of CI. Concentrations of fatty acid substrates must be optimized carefully, to reach substrate saturation without inducing inhibitory and uncoupling effects. The octanoylcarnitine concentration was 0.2 mM (39) in the present protocol. Higher concentrations did not yield higher flux.
4. Ascorbate and TMPD (Table 1) are artificial electron donors reducing cytochrome *c*. Ascorbate is added first, to maintain TMPD in a reduced state. CIII is inhibited by antimycin A or myxothiazol, to activate cytochrome *c* oxidase (CIV) as

an isolated step. Autooxidation of ascorbate and TMPD depends on (i) their concentrations, (ii) oxygen concentration, (iii) concentration of added cytochrome *c*, and (iv) the medium. Histidine stimulates autooxidation of ascorbate and is therefore omitted from MiR06. Chemical background oxygen flux plus ROX is determined at the end of an experimental run after inhibition of CIV by cyanide or azide at low oxygen concentration, continued after reoxygenation at high oxygen concentration. The keto acids pyruvate and α-ketoglutarate remove cyanide from CIV, forming the respective cyanohydrins. Reversibility of cyanide inhibition is particularly effective at high oxygen levels (40). Cyanide cannot be used, therefore, in the presence of pyruvate as a CIV inhibitor. High azide concentrations must be applied for full inhibition of CIV (Table 1). To separate autooxidation from ROX, oxygen consumption is determined in the absence of biological material under experimental conditions as a function of oxygen concentration. The chemical and instrumental background is subtracted from total measured oxygen flux to obtain CIV activity.

5. Cytochrome *c* does not pass the intact outer mt-membrane. Comparable to the succinate test for plasma membrane permeability, a cytochrome *c* test can be applied to evaluate the intactness of the outer mt-membrane in mitochondrial preparations (28). Permeabilized fibers of human v. lateralis (healthy controls) do not show any cytochrome *c* effect when 10 μM cytochrome *c* is added (Fig. 6). Cytochrome *c* is added early in the protocol (after ADP; ref. 41) to obtain all active fluxes in a comparable *c*-activated state, or at a late active state (Fig. 6; or after 100-min incubation; ref. 42), indicating stability of the outer mt-membrane. The kinetic response to external oxidized cytochrome *c* is monophasic hyperbolic and identical in cytochrome *c*-depleted permeabilized fibers and isolated mitochondria of rat heart (treated by hypo-osmotic shock), with a c_{50} of 0.4 μM cytochrome *c* supporting half-maximum flux with succinate + rotenone and saturating ADP (28, 33). 10 μM cytochrome *c*, therefore, is sufficient to saturate electron transfer from CII. In the presence of 0.5 mM TMPD and 2 mM ascorbate, the kinetic response to cytochrome *c* is biphasic, with a high-affinity K'_m of 0.5 and 0.9 μM in isolated mitochondria versus permeabilized fibers, and a low-affinity K'_m of 12 μM in both preparations. Then 10 μM cytochrome *c* saturates the velocity of CIV to only 63 and 75% in fibers and mitochondria, respectively (28, 33).

3.3.3. ADP and Inorganic Phosphate

ADP and inorganic phosphate are added to permeabilized cells and fibers at high concentrations to saturate OXPHOS capacity. The transmembrane proton pumps drive H^+ out of the matrix

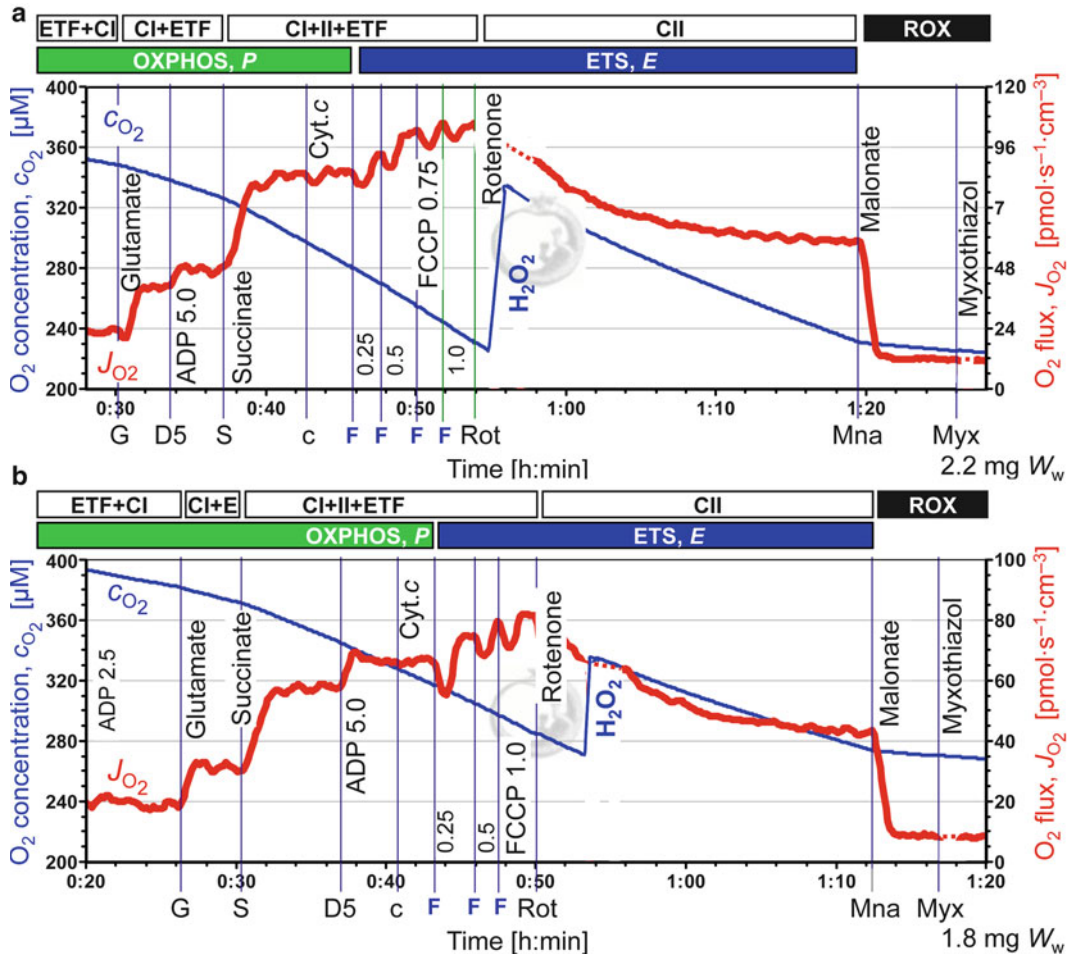

Fig. 6. Oxygen concentration (c_{O_2}) and volume-specific oxygen flux [J_{O_2} (pmol O_2 s^{-1} cm^{-3})], as a function of time, in a SUIT protocol with permeabilized human muscle fibers, with octanoylcarnitine + malate and 2.5 mM ADP, addition of glutamate (G), succinate (S), cytochrome *c* (Cyt *c*), FCCP (F), and rotenone (Rot; see Table 1). 2.5 and 5 mM ADP resulted in $J_{D_{2.5}}/J_{D_5}$ flux ratios of 0.86 for CI respiration (**a**) and CI + II respiration (**b**); $J_{D_{2.5}}/J_E$ was 0.71 and J_{D_5}/J_E was 0.82. J_{D_5}/J_E provided an estimate of the phosphorylation system control ratio (*P*/*E*). *P*/*E* was 0.80 and 0.82 with CI + II + ETF substrates (**a**, **b**). Corresponding ETS capacities at 0.75 and 1.0 µM FCCP (F; three titrations) were (**a**) *JE* = 98 pmol O_2 s^{-1} mg^{-1} W_w (2.2 mg W_w) and (**b**) 91 pmol O_2 s^{-1} mg^{-1} W_w (1.8 mg W_w). The additive effect CI + II electron-input is seen by the increase in flux after the addition of succinate and inhibition by rotenone. Reoxygenations by injections of H_2O_2 into MiR06. 37 °C, 2-ml chamber. Experiments 2010-07-12H-01 and 2010-06-24 H-01.

phase against an electrochemical backpressure, which is used in turn to fuel phosphorylation of ADP and release of ATP at the ATP synthase. The proton circuit is partially coupled in the OXPHOS state, since a fraction of the electrochemical gradient is dissipated through proton leaks. Diffusion restriction as shown by oxygen kinetics (Subheading 3.3.6) and the outer mt-membrane generate barriers for inorganic phosphate and ADP different from isolated mitochondria (2, 8, 27, 43). MiR06 contains 10 mM phosphate. Saturation by ADP requires testing by titrations. At a high apparent K_m for ADP of 0.5 mM (27), flux at 2.5 and 5 mM

ADP is ADP-limited by 13 and 7% (assuming L/P=0.2). 2.5 mM ADP is saturating in many cases, yet a further increase of ADP concentration provides a test for saturating [ADP]. This is particularly important for the evaluation of OXPHOS versus ETS capacity (P versus E; Fig. 6).

3.3.4. SUIT Protocols

Substrate combinations that match physiological intracellular conditions are applied for the evaluation of coupling control, OXPHOS, and ETS capacities. A new perspective of mitochondrial physiology and respiratory control emerged from a series of studies based on HRR with novel SUIT protocols (37, 41, 44). A SUIT protocol is shown in Fig. 7a, which may be summarized in abbreviated form. Abbreviations and sites of action are listed in Table 1. Subscripts indicate coupling control states (N: no adenylates, $D_{2.5}$ and D_5: 2.5 and 5 mM ADP; $F_{=1.25}$: stepwise titration for evaluation of optimum 1.25 μM FCCP concentration, inducing the noncoupled state E); ETS inhibitors are in parentheses:

$$\mathrm{OctM_N} + D_{2.5} + G_{D_{2.5}} + S_{D_{2.5}} + D_5 + F_{=1.25} + (\mathrm{Rot})_E + (\mathrm{Mna} + \mathrm{Myx} + \mathrm{Ama})_{\mathrm{ROX}} \quad (1)$$

1. $\mathrm{OctM_N}$: $(\mathrm{ETF} + \mathrm{CI})_L$, octanoylcarnitine (Oct) and malate (M) in the LEAK state L, in the absence of ADP (no adenylates, N).
2. $\mathrm{OctM}_{D_{2.5}}$: $(\mathrm{ETF} + \mathrm{CI})_P$, OXPHOS ($P$; State 3) after titration of 2.5 mM ADP (D), flux increases to active respiration, limited by substrate supply to ETF and CI.
3. $\mathrm{GMOct}_{D_{2.5}}$: $(\mathrm{CI} + \mathrm{ETF})_{D_{2.5}}$, stimulation by glutamate, with malate as substrates for CI; OXPHOS is ADP-limited at 2.5 mM.
4. $\mathrm{GMSOct}_{D_{2.5}}$: $(\mathrm{CI} + \mathrm{II} + \mathrm{ETF})_{D_{2.5}}$, respiration is further stimulated by adding succinate, activating convergent electron flow from CI + II into the Q-cycle (4, 37).
5. GMSOct_{D_5}: $(\mathrm{CI} + \mathrm{II} + \mathrm{ETF})_P$, OXPHOS capacity at 5 mM ADP.
6. GMSOct_E: $(\mathrm{CI} + \mathrm{II} + \mathrm{ETF})_E$, ETS capacity after FCCP titration in steps of 0.5, 1.0, and 1.25 μM optimal concentration (noncoupled state). Activation by uncoupling is expected if the phosphorylation system (ANT, ATP synthase, phosphate transporter) limits OXPHOS capacity (4, 37), but also if ADP is not saturating.
7. $\mathrm{S(Rot)}_E$: CII_E, after inhibition of CI by rotenone, ETS capacity is measured with the entry of electrons from CII only into the Q-cycle.
8. $(\mathrm{Mna} + \mathrm{Myx} + \mathrm{Ama})_{\mathrm{ROX}}$: ROX is determined after sequential inhibition of the ETS by malonic acid (CII), myxothiazol, and antimycin A (CIII).

As shown in the coupling/substrate control diagram (Fig. 7c), alternative protocols are required with separate incubations to obtain information on additional coupling/substrate states. Protocol (2) starts again in state $(\mathrm{ETF} + \mathrm{CI})_L$, then places emphasis

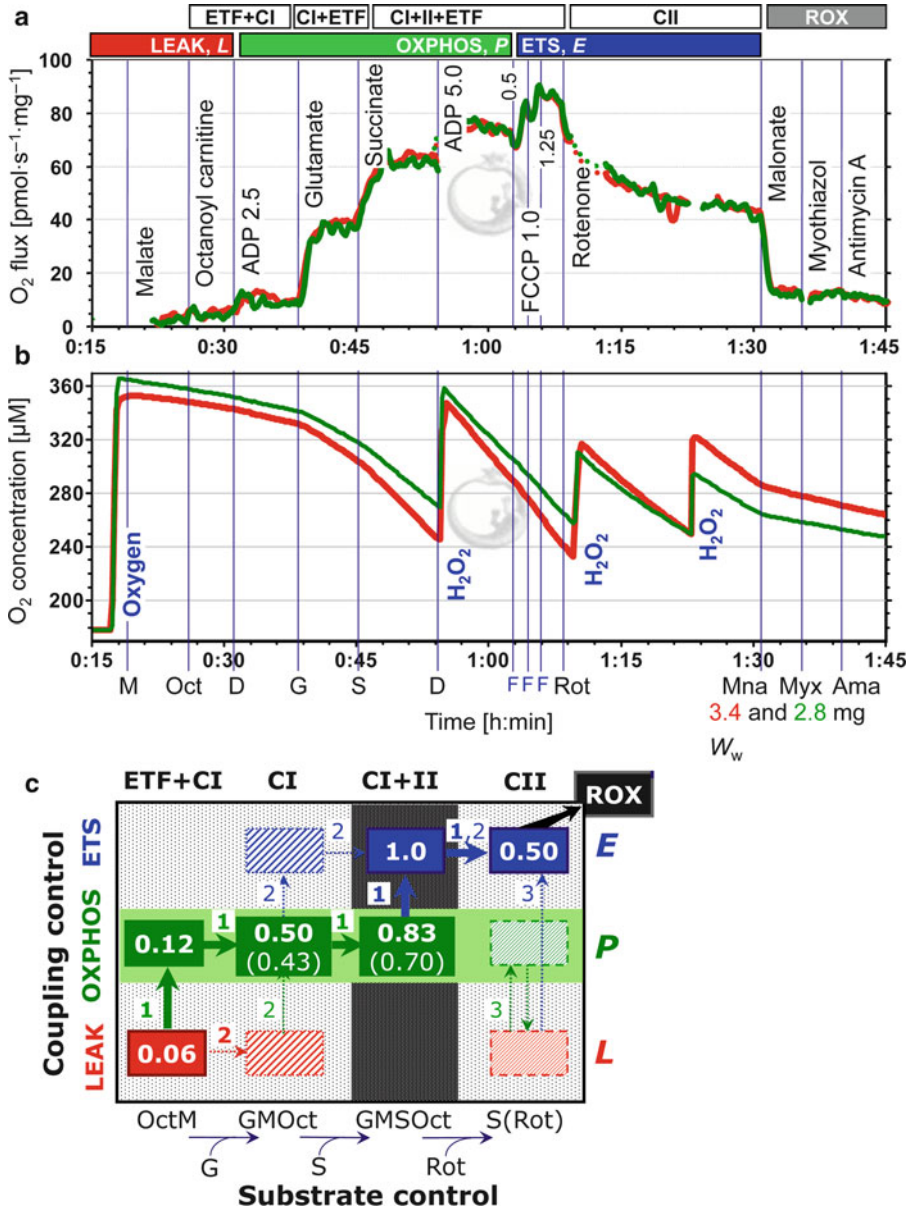

Fig. 7. Substrate–uncoupler–inhibitor titration (SUIT) protocol with substrates for electron-transferring flavoprotein (ETF), Complex I (CI), and Complex II (CII). See also Fig. 5. (**a**, **b**) Superimposed oxygraph traces from parallel measurements in two chambers with permeabilized fibers from a biopsy of human vastus lateralis, 3.4 and 2.8 mg W_w. (**a**) Mass-specific oxygen flux (pmol $O_2 s^{-1}$ mg^{-1} W_w). (**b**) Oxygen concentration (µmol/dm^3). Oxygen flux is not shown during a few minutes after oxygenations by oxygen or hydrogen peroxide, when the calculation of slopes is disturbed by the step changes in oxygen concentration. 37 °C, MiR06, 2-ml chamber. Experiment 2010-03-04 CD-01. (**c**) Coupling/substrate control diagram with flux control ratios (FCRs) normalized relative to ETS capacity with convergent CI + II electron input (*arrows 1*, corresponding to Fig. 6a; *FCRs* in parentheses are pseudo-state *P** at 2.5 mM ADP). Additional protocols (*arrows 2* and *3*) are required to fill in the dashed coupling/substrate states, including overlapping respiratory state $S(Rot)_E$ in all cases. Residual oxygen consumption (ROX) is determined as a common step in the three protocols on integrated pathways.

on coupling control with CI substrates from $(CI+ETF)_L$, $(CI+ETF)_P$, to $(CI+ETF)_E$, and finally on substrate control with $(CI+II+ETF)_E$ and CII_E. A cytochrome *c* test (+c; Fig. 6) is added:

$$OctM_N + G_N + D_P + c_P + F_E + S_E + (Rot)_E + (Mna + Myx + Ama)_{ROX} \quad (2)$$

Protocol (3) represents a sequence of coupling states at constant substrate supply with CII electron input, *S*(Rot), from CII_L, CII_P, back to CII_L (+Omy), to CII_E, and ROX:

$$S(Rot)_N + D_P + Omy_L + F_E + (Mna + Myx + Ama)_{ROX} + AsTm_E + (Kcn)_{ROX'} \quad (3)$$

For illustration, measurements are added of CIV activity (+AsTm) and chemical background (ROX′ includes autooxidation after inhibition by KCN; Table 1).

In the design of multiple, complementary protocols, it is important to include one or several overlapping coupling/substrate states, providing a quantitative link between the separate experimental incubations (Fig. 7c).

3.3.5. Oxygen Flux, Normalization of Flux, and Flux Control Ratios

Mass-specific flux of permeabilized muscle fibers is expressed per mg wet weight (Fig. 7a), integrating mitochondrial quality and quantity (mt-density). Rather than tabulating mitochondrial respiration in an unnecessary variety of units, SI units provide a standard for expressing oxygen flow (mol $O_2\,s^{-1}$; pmol/s) (Table 2) and mass-specific oxygen flux (pmol/s per mg). Multiply "bioenergetic" units (ng atom O min^{-1}) by 8.33 to convert to SI units (pmol $O_2\,s^{-1}$).

To separate the effects of mt-quality from mt-density, a common mt-marker is used for normalization, such as mtDNA (41), citrate synthase activity or CIV activity (12), or cytochrome aa_3 content (8). Subsamples or the entire contents can be collected from the O2k-chamber for the analysis of CS activity (29). Respiratory flux control ratios, FCR (Fig. 7c), however, are internal ratios within an experimental run and thus minimize several experimental errors, providing the most powerful normalization of flux (4). Substrate control ratios are FCR at constant coupling state, whereas coupling control ratios are FCR at constant substrate state, relating *L* and *P* to *E* (Fig. 7c).

1. The LEAK control ratio, *L*/*E*, expresses uncoupling or dyscoupling, provided that specific limitations of flux by *E* are considered. *L*/*E* increases with uncoupling from a theoretical minimum of 0.0 for a fully coupled system to 1.0 for a fully dyscoupled state.
2. The phosphorylation system control ratio, *P*/*E*, increases from a minimum of *L*/*E* if the capacity of the phosphorylation system is zero to the maximum of 1.0 if the capacity of the phosphorylation system fully matches the ETS capacity (or in

fully dyscoupled mitochondria), when there is no limitation of P by the phosphorylation system or the proton backpressure. It is important to separate the effect of ADP limitation from limitation by enzymatic capacity at saturating ADP concentration (Fig. 6). In Fig. 7, the P/E flux ratio was 0.83 at 5 mM ADP, whereas the pseudo-state P control ratio (P^*/E) was 0.70 at 2.5 mM ADP, due to ADP limitation of respiration.

3. The conventional respiratory control ratio, RCR (State 3/State 4 or P/L) increases from 1.0 to infinity from fully dyscoupled to fully coupled mitochondria. But the RCR declines with increasing levels of coupling as a function of the phosphorylation system control ratio, P/E. For mathematical reasons, it is more appropriate to use the inverse RCR, which is the L/P ratio with the theoretical boundaries of 0.0 at tight coupling, to the maximum of $(L/E)/(P/E) \leq 1.0$, which becomes 1.0 in fully dyscoupled mitochondria. The RCR is useful only in the limiting case when the P/E ratio is 1.0 (since then $L/P = L/E$; ref. 4).

3.3.6. Oxygen

Physiological intracellular oxygen levels are significantly lower than air saturation under normoxia, hence respiratory measurements carried out at air saturation are effectively hyperoxic for cultured cells and isolated mitochondria (10). Respiratory capacity, however, of mitochondrial preparations must be evaluated at kinetic oxygen saturation as a reference state. The apparent K_m for oxygen (c_{50} [μM] or p_{50} (kPa) is controlled by diffusion gradients and metabolic state. Even at 20 μM, oxygen does not limit respiration of isolated mitochondria and small cells (20- to 50-fold above the c_{50} of 0.4–1.0 μM (32–34)). In permeabilized muscle fiber bundles, however, diffusion restriction increases the sensitivity to oxygen supply to a c_{50} of 10 μM in the passive LEAK state of respiration, when diffusion gradients are small at low oxygen flux. In the active ADP-stimulated state, the c_{50} is increased to 40 μM, or 100-fold above that of isolated mitochondria (30 °C; rat soleus and rat heart, incubated with pyruvate and malate (5, 45)). Similarly, oxygen limitation of respiration in permeabilized fibers from human v. lateralis is significant at all levels below air saturation, with a typical c_{50} of 50 μM for ADP-stimulated respiration (37 °C; Figs. 8 and 9). For the analysis of oxygen kinetics, respiration is monitored during aerobic–anaerobic transitions (Fig. 8a) and plotted as a function of oxygen concentration (Fig. 8b). In many but not all cases, a hyperbolic function provides a good fit (Fig. 8b). Instability of respiration over prolonged periods of incubation time may distort the oxygen kinetics, which is minimized by using larger amounts of tissue in such tests, and evaluated by observation of recovery of oxygen flux after reoxygenation (Fig. 8a). Extrapolation of a hyperbolic relationship below air saturation (Fig. 8b) does not appear to be valid, as seen by the constant flux after reoxygenation (Fig. 8a).

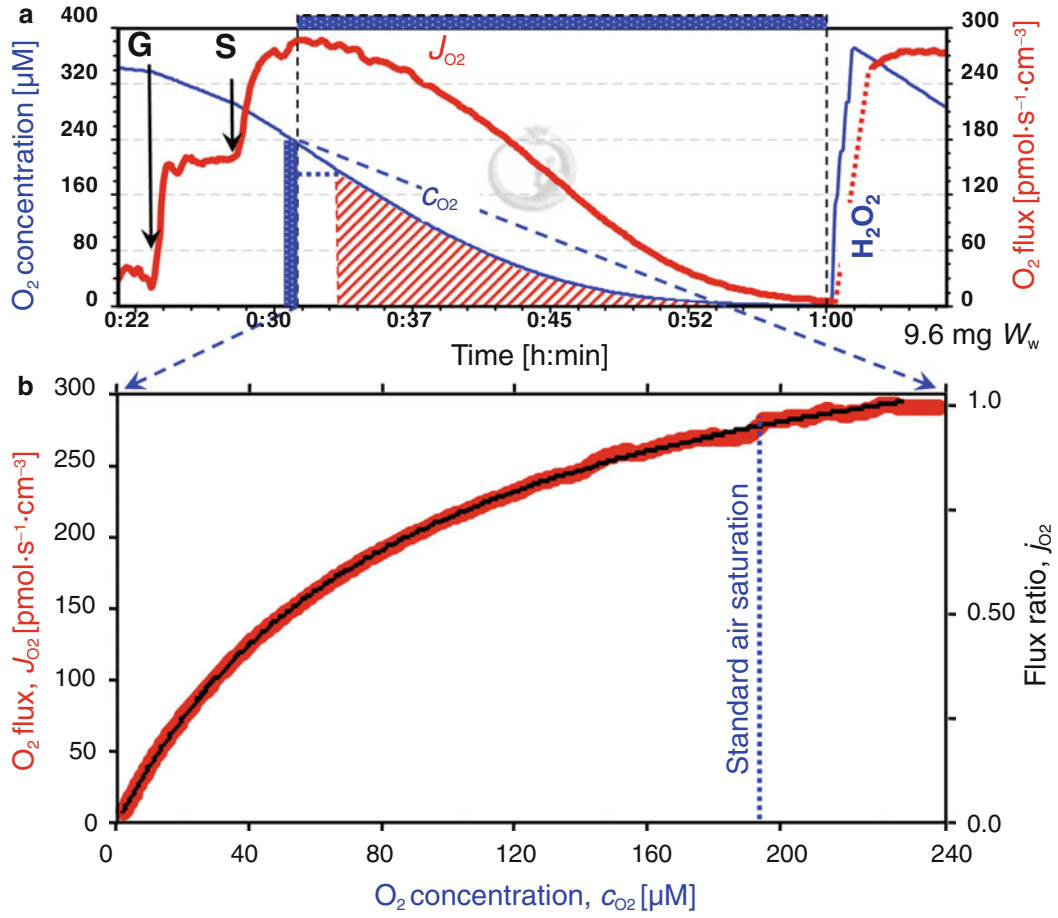

Fig. 8. Oxygen dependence of respiration of permeabilized fibers (human vastus lateralis, 9.6 mg W_w). (**a**) Online traces of oxygen concentration (c_{O_2}; range 0–400 µM), and volume-specific flux (J_{O_2}). Malate and 2.5 mM ADP, addition of glutamate (G), succinate (S), reoxygenation with H_2O_2 after 1-h incubation, indicating stability of respiration at high oxygen levels. The region of oxygen-conformance of respiration is shown by the hatched area. (**b**) Kinetic plot of volume-specific oxygen flux (J_{O_2}) or flux ratio (j_{O_2} ; normalized relative to flux at 240 µM), as a function of oxygen concentration; hyperbolic fit is indistinguishable from the measured data points (p_{50} of 5.2 kPa, c_{50} of 50 µM O_2), in the first phase of declining oxygen concentration (stippled range in panel **a**). 37 °C, MiR06, 2-ml chamber. Experiment 2010-02-26 D-01.

Multiphasic oxygen kinetics becomes particularly evident in cases when the muscle fiber bundle (Fig. 9a) is mechanically separated further into many small pieces during stirring in the O2k-chamber (Fig. 9b). In the latter case, the oxygen diffusion distance is reduced for an increasing fraction of mitochondria, such that the last phase in the aerobic–anaerobic transition resembles that of isolated mitochondria with a steep decline of flux toward oxygen exhaustion (compare Fig. 9a, b).

In summary, elevation of oxygen levels in respirometry with permeabilized muscle fibers is necessary to avoid the development of an artificial hypoxic or anoxic core in the nonperfused fiber bundle (see Note 3). The high degree of oxyconformance in permeabilized

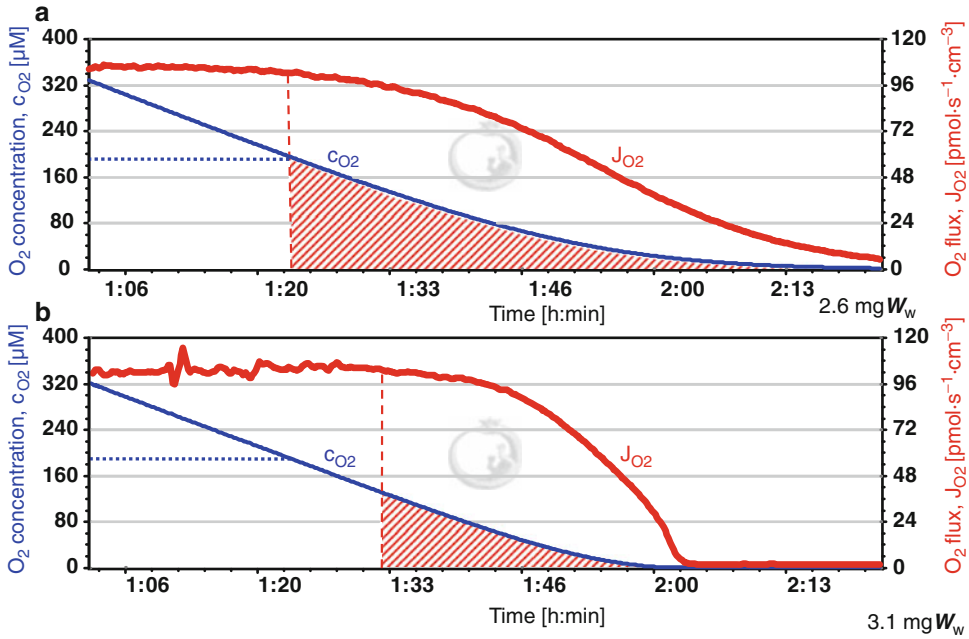

Fig. 9. Oxygen dependence of respiration in two parallel experiments with samples from a biopsy of human vastus lateralis, 2.6 and 3.1 mg W_w (**a**, **b**). The *horizontal dotted lines* indicate the oxygen concentration of 191 µM corresponding to air saturation at standard pressure (100 kPa; 19.6 kPa partial oxygen pressure). (**a**) Typical near-hyperbolic oxygen dependence, with an apparent p_{50} of 5.4 kPa (c_{50} of 52 µM O_2; but nonhyperbolic extension at high oxygen; compare Fig. 8). (**b**) Multiphasic oxygen dependence in fibers that were disrupted into small pieces by the stirrer in the chamber, without inducing turbidity. The last phase at lowest oxygen levels indicates an apparent p_{50} equivalent to the kinetics of isolated mitochondria, whereas the first phase at high oxygen levels reflects the oxygen dependence of intact permeabilized fibers. 37 °C, MiR06, 2-ml chamber. Experiment 2010-04-26 GH-01.

fibers is not a kinetic property of the mitochondria, but is largely determined by the geometry of the fiber bundle, with diffusion distances increased from 5–10 µm in cells to >150 µm in the intertwined bundle (5). As a consequence, a compromise is suggested to maintain oxygen levels in the range >250 µM to minimize oxygen limitation of respiration, but <500 µM to avoid extremes of hyperoxia experienced by the peripheral or partially separated mitochondria in the oxygraph chamber.

1. Add 2.2-ml medium into the chamber and insert the stopper incompletely, leaving an air space above the stirred medium. A stopper spacer is used for optimal and reproducible positioning. In this state, the oxygen sensors are air-calibrated (Subheading 3.4.1) while fibers are permeabilized. Remove the stopper, insert a permeabilized fiber bundle into the medium, and insert the stopper incompletely. Inject a few milliliters of oxygen from a gas injection syringe through a needle inserted into the injection port of the stopper and extending into the gas phase, but not into the aqueous phase. Thereby an elevated

oxygen pressure is created above the stirred aqueous medium. Oxygen in the gas and aqueous phases starts to equilibrate rapidly. When the desired oxygen concentration above 400 μM is nearly reached, close the chamber, thereby removing the gas phase and stopping the equilibration process.

2. Small reoxygenation steps during the experiment can be performed by titrating a few microliters of H_2O_2 (200 mM in H_2O, adjust to pH 6 and keep on ice to minimize autooxidation) into MiR06 (containing catalase). This is sufficient to raise oxygen levels from 250 μM again to 400 μM. After injecting H_2O_2, the time required for the flux to stabilize depends on the step change of oxygen; smaller steps require less time for stabilization (Figs. 6 and 7). Using H_2O_2 increases total gas pressure with oxygen pressure. This can generate bubbles in steps from air saturation to >400 μM, that is why O_2 gas is applied initially.

3.4. High-Resolution Respirometry

3.4.1. Calibration of the Polarographic Oxygen Sensor

Dissolved oxygen concentration is measured amperometrically by Clark-type polarographic oxygen sensors (POS), containing a gold cathode and Ag/AgCl anode connected electrically by a KCl electrolyte, and separated from the sample by an O_2-permeant FEP membrane (0.25 μm). A polarization voltage of 0.8 V is applied to reduce O_2 that diffuses from the incubation medium to the cathode through the membrane. O_2 is reduced to water, generating a current (hence amperometric) that is linearly proportional to O_2 partial pressure, P_{O_2}, in the stirred experimental solution (46). After current-to-voltage conversion and amplification, the raw signal is obtained (1 V/μA; with further amplification by gain settings of 2 or 4). Data sampling at time intervals of 2 s is sufficient for routine applications, 1 s is recommended for kinetic experiments, and it can be reduced to 0.2 s for applications with high sample concentrations. 100 data points are averaged at each data sampling interval. The limit of detection of oxygen concentration extends to 0.005 μM (5 nM) O_2. The digital resolution is 2 nM, yielding a 500,000-fold dynamic range up to oxygen saturation. The polarographic oxygen sensors (OROBoPOS) are stable for several months without exchange of membranes or electrolyte (3). A standardized calibration of the linear oxygen sensor includes quality control of signal stability (noise and drift; static two-point sensor calibration) and dynamic calibration of the sensor response time (2).

1. For storage, fill up the clean O2k-chambers completely with 70% ethanol, with the POS and stirrers remaining in the assembled chamber, and the stopper loosely inserted and covered by a lid. Storage in 70% ethanol between experiments can be extended over periods of months, keeping the chamber sterile and the POS immediately ready to use (3).
2. After switching on the instrument, set the experimental temperature, wash with distilled or deionized water while the

stirrer is on (750 rpm or 12.5 Hz is optimal), and add 2.2-ml experimental medium (MiR06). Insert the stoppers slowly to their volume-calibrated position (2-ml effective volume, plus 0.08 ml to fill the stopper capillary). Siphon off excess medium ejected through the stopper capillary with the integrated suction system (ISS; Fig. 1).

3. Lift the stoppers slightly to introduce an air space above the stirred aqueous medium (open position with stopper spacer), and allow for sufficient time to obtain temperature stability and oxygen equilibration between the gas and aqueous phases. The gas volume has to be exchanged for air, if the medium has not been near air saturation initially, to ensure a well-defined p_{O_2} in the gas phase during air equilibration. Equilibration is a slow process, but stability should be reached within 30–60 min.
4. During this time, a quick stirrer test is performed for dynamic sensor calibration, switching off the stirrer shortly with the consequence of a sharp drop of the POS signal, and observing the exponential increase of the signal after the stirrer is switched on. The corresponding response time is a sensitive indicator of dynamic sensor performance, and deconvolution of the signal is possible for high time resolution in kinetic studies (1, 2, 10).
5. The signal at air saturation provides the first calibration point, with raw signal R_1. During this period, the slope of O_2 over time must be less than 0.5–1.0 pmol/s per ml, indicating proper signal stability of the POS. Air calibrations are performed daily before starting an experiment (47).
6. Titrate 100 µl freshly prepared 10 mM solution of sodium dithionite to fully exhaust the dissolved oxygen concentration to zero. The zero signal, R_0, should be <3% of R_1, but most importantly, R_0 must be stable (higher stability and lower noise than at air saturation). Occasional checks over a period of months are sufficient (3), except in studies of oxygen kinetics, when short-term zero drift must be accounted for by internal zero calibration after oxygen depletion by mitochondrial respiration, for resolution in the nanomolar oxygen range (1, 2, 10, 34).

3.4.2. Oxygen Solubility and Concentration

To convert p_{O_2} [kPa] to oxygen concentration c_{O_2} [µM], the oxygen solubility of the medium is calculated as a function of temperature and salt concentration. Oxygen calibration is fully supported by the OROBOROS DatLab software and combines the following information (47):

1. Raw signal [R_1 (V)] obtained at air saturation of the medium.
2. Raw signal [R_0 (V)] obtained at zero oxygen concentration.
3. Experimental temperature [T (°C)] measured in the thermoregulated copper block (Fig. 1).

4. Barometric pressure [p_b (kPa)] measured by an electronic pressure transducer.
5. The oxygen partial pressure [p_{O_2} (kPa)] in air saturated with water vapor, as a function of barometric pressure and temperature, calculated by the DatLab software (46).
6. The oxygen solubility [S_{O_2} (μM/kPa)] in pure water as a function of temperature, calculated by the DatLab software (46).
7. The oxygen solubility factor of the incubation medium (F_M) which expresses the effect of the salt concentration on oxygen solubility relative to pure water. In MiR06, F_M is 0.92 determined at 30 and 37 °C, and F_M is 0.89 in serum at 37 °C. The same factor of 0.89 can be used for various culture media such as RPMI (47). At standard barometric pressure (100 kPa), the oxygen concentration at air saturation is 207.3 μM at 37 °C (19.6 kPa partial oxygen pressure; (46)). In MiR06 and serum, the corresponding saturation concentrations are 191 and 184 μM, respectively.

3.4.3. Oxygen Flux and Instrumental Background

Long-term signal stability and low noise of the oxygen signal are a basis for online display of oxygen flux calculated as the negative time derivative of oxygen concentration. The limit of detection in HRR of oxygen flux is 1 pmol/s per cm³ (0.001 μM/s). With small amounts of sample and correspondingly low respiratory flux per volume, the oxygen capacity of the system provides sufficient time to evaluate the stability of respiratory activity in each metabolic state and to permit complex titration regimes (Fig. 7). At a constant volume-specific flux of 100 pmol/s per cm³, 180 μM O_2 is exhausted within 30 min (Fig. 7b).

Oxygen consumption by the POS and oxygen diffusion below or above air saturation contribute to instrumental background oxygen flux, which is minimized in HRR and corrected for (1–3). At air saturation, the POS generates a current of about 2 μA at a stoichiometry of four electrons/O_2. The O_2/electron ratio divided by the Avogadro constant (F=96,485.53 C/mol) yields the amount of oxygen per Coulomb [$1/(4 \cdot F) = 2.591$ μmol O_2 C^{-1}] or O_2 flow per current (2.591 pmol/s per μA). At 2 μA per 2 ml, therefore, volume-specific O_2 flux or O_2 consumption by the POS ($J_{O_2,POS}$) is 2.6 pmol/s per ml. $J_{O_2,POS}$ declines to zero as a strictly linear function of p_{O_2} or c_{O_2} under constant experimental conditions. Hence correction for $J_{O_2,POS}$ is simple and accurate, and does not influence the limit of detection of biological flux. In contrast, the contribution of oxygen diffusion to instrumental background is unpredictable in various respirometric systems, and needs to be determined empirically in the closed chamber in the absence of biological material, as a function of oxygen concentration in the experimental range. Effects of oxygen back-diffusion are minimized

in the Oxygraph-2k by the large volume (2 ml) and the selection of diffusion-tight materials in contact with the respiration medium: Glass chambers and PVDF or titanium stoppers (not Perspex), magnetic stirrer bars coated by PVDF or PEEK (not Teflon), and Viton O-rings (not silicon). Compared to aqueous media, plastic materials such as Teflon have a >10-fold higher oxygen solubility. Plastic is not feasible for respirometry, since uncontrolled oxygen back-diffusion distorts the respiratory decline of oxygen concentration in a closed chamber.

Instrumental background tests were designed to detect and eliminate possible oxygen leaks, introducing this integrated systemic calibration as a key component of quality control in HRR ((1–3, 48); see Note 4).

1. Close the chamber by fully inserting the stoppers after stabilization at air saturation, excluding any gas bubbles. After 10–15 min, observe instrumental background flux (J°_1) which is due to $J_{O_2,POS}$ only. $J_{O_2,POS}$ is 2.5–3.5 pmol/s per cm³ at air saturation in the 2-ml O2k-chamber at 37 °C. Agreement with the predicted flux validates the instrumental limit of detection of flux. Higher J°_1 is due to microbial contamination of the medium and chamber. J°_1 would increase to 25 pmol/s per cm³ in a 200-µl chamber. Whereas $J_{O_2,POS}$ decreases linearly to zero at anoxia, it increases to 8 pmol/s per cm³ at 500 µM O_2, but instrumental background flux J_{O_2} does not conform to $J_{O_2,POS}$ at these oxygen levels.

2a. Lower experimental oxygen concentrations are obtained by stepwise titration of small volumes of freshly prepared 10 mM solution of sodium dithionite ($Na_2S_2O_4$; 1.7 mg/ml phosphate buffer, pH 8) into MiR06. Standardized four-step background tests (J_{O_2} at air saturation, 100, 50, and 20 µM O_2) can be performed automatically using the programmed OROBOROS Titration-Injection microPump (TIP2k; ref. 48). Alternatively, the chamber is opened intermittently for flushing the gas phase with nitrogen or argon, and closed at reduced oxygen concentration. The near-linear dependence of $J^{\circ}_{O_2}$ on oxygen concentration extrapolates to zero oxygen concentration with an intercept a° of –1.5 to –2.5 pmol/s per cm³, which is the oxygen back-diffusion per volume of the chamber at zero oxygen concentration. A typical value of the slope b° is 0.025. More negative values of a° indicate an oxygen leak in the system.

2b. In experiments with permeabilized fibers at elevated oxygen levels, instrumental background is measured in the experimental range after increasing the oxygen concentration in MiR06 (see above), and stepwise measurement of $J^{\circ}_{O_2}$ at four oxygen levels matching the experimental oxygen regime (Fig. 7b: 370,

330, 300, and 240 μM). The recommended range is 400–250 μM.

3. Plot $J^{\circ}_{O_2}$ as a function of average c_{O_2} during the period of determining $J^{\circ}_{O_2}$.Calculate a° and b° by linear regression (DatLab), $J^{\circ}_{O_2} = a^{\circ} + b^{\circ} \times c_{O_2}$.
4. Background-corrected volume-specific oxygen consumption [J_{V,O_2} (pmol/s per cm³)] is calculated automatically for each data point (DatLab, online) over the entire experimental oxygen range (1–3),

$$J_{V,O_2} = -\frac{dc_{O_2}}{dt} \times 1,000 - \left(a^{\circ} + b^{\circ} \times c_{O_2}\right) \quad (3.4)$$

where c_{O_2} (μM or nmol/cm³) is oxygen concentration measured at time t, dc_{O_2}/dt is the time derivative of oxygen concentration, and the expression in parentheses is instrumental background oxygen flux.

4. Notes

1. OXPHOS protocols presented in this chapter and instrumental standards in HRR address new challenges in mitochondrial respiratory physiology and pathology.
2. Emphasis is placed on intact cells, permeabilized cells, and permeabilized muscle fibers. It has not been shown if isolation of mitochondria involves the selective loss of damaged mitochondria, but in any case all types of mitochondria are accessible experimentally in permeabilized cells and tissues. Respiration of permeabilized skeletal muscle fibers and isolated mitochondria yields comparable results on OXPHOS capacity (4).
3. A recent methodological presentation of respirometry with permeabilized muscle fibers (49) lacks consideration on oxygen limitation summarized previously (45, 50), tabulates respiration of rat liver homogenate at 30 °C (49) which is actually mechanically permeabilized pig liver measured at 37 °C (29), and restricts discussion of protocols to simple substrate supply (separate CI- or CII-electron entry into the ETS), whereas full OXPHOS capacity can be obtained only with physiological CI + II substrate combinations (4, 30, 37, 41, 42, 44).
4. Demands are increasing for quality control, quality assurance, traceability of calibrations, and standardization of protocols for functional mitochondrial diagnosis in biomedical research and clinical applications.

Acknowledgments

This work was supported by OeNB Jubiläumsfond project 13476 and is a contribution to Mitofood COST Action FAO602. We thank Dr. Michael Schocke who was responsible for taking the human biopsies, and Drs. Robert Boushel, Flemming Dela, Steen Larson, Nis Stride, Dan Kane, and Darrel Neufer for advice in the technique of biopsy sampling.

References

1. Gnaiger E, Steinlechner-Maran R, Méndez G, Eberl T, Margreiter R (1995) Control of mitochondrial and cellular respiration by oxygen. J Bioenerg Biomembr 27:583–596
2. Gnaiger E (2001) Bioenergetics at low oxygen: dependence of respiration and phosphorylation on oxygen and adenosine diphosphate supply. Respir Physiol 128:277–297
3. Gnaiger E (2008) Polarographic oxygen sensors, the oxygraph and high-resolution respirometry to assess mitochondrial function. In: Dykens JA, Will Y (eds) Mitochondrial dysfunction in drug-induced toxicity. Wiley, New York, pp 327–352
4. Gnaiger E (2009) Capacity of oxidative phosphorylation in human skeletal muscle. New perspectives of mitochondrial physiology. Int J Biochem Cell Biol 41:1837–1845
5. Gnaiger E (2003) Oxygen conformance of cellular respiration: a perspective of mitochondrial physiology. Adv Exp Med Biol 543:39–56
6. Gnaiger E, Kuznetsov AV, Schneeberger S, Seiler R, Brandacher G, Steurer W, Margreiter R (2000) Mitochondria in the cold. In: Heldmaier G, Klingenspor M (eds) Life in the cold. Springer, New York, pp 431–442
7. Fasching M, Renner-Sattler K, Gnaiger E (2010) Mitochondrial respiration medium – MiR06. Mitochondr Physiol Netw 14(13): 1–4. http://www.oroboros.at
8. Veksler VI, Kuznetsov AV, Sharov VG, Kapelko VI, Saks VA (1987) Mitochondrial respiratory parameters in cardiac tissue: a novel method of assessment by using saponin-skinned fibers. Biochim Biophys Acta 892:191–196
9. Skladal D, Sperl W, Schranzhofer R, Krismer M, Gnaiger E, Margreiter R, Gellerich FN (1994) Preservation of mitochondrial functions in human skeletal muscle during storage in high energy preservation solution (HEPS). In: Gnaiger E, Gellerich FN, Wyss M (eds) What is controlling life? vol 3, Modern Trends in Biothermokinetics. Innsbruck University Press, Innsbruck, pp 268–271
10. Gnaiger E, Méndez G, Hand SC (2000) High phosphorylation efficiency and depression of uncoupled respiration in mitochondria under hypoxia. Proc Natl Acad Sci USA 97: 11080–11085
11. Steinlechner-Maran R, Eberl T, Kunc M, Margreiter R, Gnaiger E (1996) Oxygen dependence of respiration in coupled and uncoupled endothelial cells. Am J Physiol 271:C2053–C2061
12. Renner K, Amberger A, Konwalinka G, Kofler R, Gnaiger E (2003) Changes of mitochondrial respiration, mitochondrial content and cell size after induction of apoptosis in leukemia cells. Biochim Biophys Acta 1642:115–123
13. Steinlechner-Maran R, Eberl T, Kunc M, Schröcksnadel H, Margreiter R, Gnaiger E (1997) Respiratory defect as an early event in preservation/reoxygenation injury in endothelial cells. Transplantation 63:136–142
14. Stadlmann S, Rieger G, Amberger A, Kuznetsov AV, Margreiter R, Gnaiger E (2002) H_2O_2-mediated oxidative stress versus cold ischemia-reperfusion: mitochondrial respiratory defects in cultured human endothelial cells. Transplantation 74:1800–1803
15. Hütter E, Renner K, Pfister G, Stöckl P, Jansen-Dürr P, Gnaiger E (2004) Senescence-associated changes in respiration and oxidative phosphorylation in primary human fibroblasts. Biochem J 380:919–928
16. Hütter E, Unterluggauer H, Garedew A, Jansen-Dürr P, Gnaiger E (2006) High-resolution respirometry – a modern tool in aging research. Exp Gerontol 41:103–109
17. Aguirre E, Rodríguez-Juárez F, Bellelli A, Gnaiger E, Cadenas S (2010) Kinetic model of the inhibition of respiration by endogenous nitric oxide in intact cells. Biochim Biophys Acta. doi:10.1016/j.bbabio.2010.01.033
18. Chance B, Williams GR (1955) Respiratory enzymes in oxidative phosphorylation. I. Kinetics of oxygen utilization. J Biol Chem 217: 383–393

19. Stadlmann S, Renner K, Pollheimer J, Moser PL, Zeimet AG, Offner FA, Gnaiger E (2006) Preserved coupling of oxidative phosphorylation but decreased mitochondrial respiratory capacity in IL-1β treated human peritoneal mesothelial cells. Cell Biochem Biophys 44:179–186
20. Smolková K, Bellance N, Scandurra F, Génot E, Gnaiger E, Plecitá-Hlavatá L, Ježek P, Rossignol R (2010) Mitochondrial bioenergetic adaptations of breast cancer cells to aglycemia and hypoxia. J Bioenerg Biomembr. doi:10.1007/s10863-009-9267-x
21. Jones DP (1986) Intracellular diffusion gradients of O_2 and ATP. Am J Physiol 250:C663–C675
22. Villani G, Attardi G (1997) In vivo control of respiration by cytochrome *c* oxidase in wild-type and mitochondrial DNA mutation-carrying human cells. Proc Natl Acad Sci USA 94:1166–1171
23. Gnaiger E, Rieger G, Kuznetsov A, Fuchs A, Stadlmann S, Lassnig B, Hengster P, Eberl T, Margreiter R (1997) Mitochondrial ischemia-reoxygenation injury and plasma membrane integrity in human endothelial cells. Transplant Proc 29:3524–3526
24. Gnaiger E, Kuznetsov AV, Rieger G, Amberger A, Fuchs A, Stadlmann S, Eberl T, Margreiter R (2000) Mitochondrial defects by intracellular calcium overload versus endothelial cold ischemia/reperfusion injury. Transpl Int 13:555–557
25. Vercesi AE, Bernardes CF, Hoffmann ME, Gadelha FR, Docampo R (1991) Digitonin permeabilization does not affect mitochondrial function and allows the determination of the mitochondrial membrane potential of *Trypanosoma cruzi* in situ. J Biol Chem 266:14431–14434
26. Gnaiger E, Kuznetsov AV, Lassnig B, Fuchs A, Reck M, Renner K, Stadlmann S, Rieger G, Margreiter R (1998) High-resolution respirometry. Optimum permeabilization of the cell membrane by digitonin. In: Larsson C, Påhlman I-L, Gustafsson L (eds) Biothermokinetics in the post genomic era. Chalmers Reproservice, Göteborg, pp 89–95
27. Saks VA, Veksler VI, Kuznetsov AV, Kay L, Sikk P, Tiivel T, Tranqui L, Olivares J, Winkler K, Wiedemann F, Kunz WS (1998) Permeabilised cell and skinned fiber techniques in studies of mitochondrial function in vivo. Mol Cell Biochem 184:81–100
28. Kuznetsov AV, Schneeberger S, Seiler R, Brandacher G, Mark W, Steurer W, Saks V, Usson Y, Margreiter R, Gnaiger E (2004) Mitochondrial defects and heterogeneous cytochrome *c* release after cardiac cold ischemia and reperfusion. Am J Physiol Heart Circ Physiol 286:H1633–H1641
29. Kuznetsov AV, Strobl D, Ruttmann E, Königsrainer A, Margreiter R, Gnaiger E (2002) Evaluation of mitochondrial respiratory function in small biopsies of liver. Anal Biochem 305:186–194
30. Rasmussen UF, Rasmussen HN (2000) Human quadriceps muscle mitochondria: a functional characterization. Mol Cell Biochem 208:37–44
31. Palmer JW, Tandler B, Hoppel CL (1977) Biochemical properties of subsarcolemmal and interfibrillar mitochondria isolated from rat cardiac muscle. J Biol Chem 252:8731–8739
32. Gnaiger E, Lassnig B, Kuznetsov AV, Margreiter R (1998) Mitochondrial respiration in the low oxygen environment of the cell: effect of ADP on oxygen kinetics. Biochim Biophys Acta 1365:249–254
33. Gnaiger E, Kuznetsov AV (2002) Mitochondrial respiration at low levels of oxygen and cytochrome *c*. Biochem Soc Trans 30:252–258
34. Scandurra FM, Gnaiger E (2010) Cell respiration under hypoxia: facts and artefacts in mitochondrial oxygen kinetics. Adv Exp Med Biol 662:7–25
35. Dubowitz V, Sewry CA (2006) Muscle biopsy: a practical approach. Saunders Elsevier, Philadelphia
36. Dufour S, Rousse N, Canioni P, Diolez P (1996) Top-down control analysis of temperature effect on oxidative phosphorylation. Biochem J 314:743–751
37. Gnaiger E (ed) (2007) Mitochondrial pathways and respiratory control. OROBOROS MiPNet, Innsbruck. http://www.oroboros.at
38. Sun F, Huo X, Zhai Y, Wang A, Xu J, Su D, Bartlam M, Rao Z (2005) Crystal structure of mitochondrial respiratory membrane protein Complex II. Cell 121:1043–1057
39. Puchowicz MA, Varnes ME, Cohen BH, Friedman NR, Kerr DS, Hoppel CL (2004) Oxidative phosphorylation analysis: assessing the integrated functional activity of human skeletal muscle mitochondria – case studies. Mitochondrion 4:377–385
40. Delhumeau G, Cruz-Mendoza AM, Lojero CG (1994) Protection of cytochrome *c* oxidase against cyanide inhibition by pyruvate and α-ketoglutarate: effect of aeration in vitro. Toxicol Appl Pharmacol 126:345–351
41. Boushel R, Gnaiger E, Schjerling P, Skovbro M, Kraunsøe R, Dela F (2007) Patients with type 2 diabetes have normal mitochondrial function in skeletal muscle. Diabetologia 50:790–796

42. Gnaiger E, Wright-Paradis C, Sondergaard H et al (2005) High-resolution respirometry in small biopsies of human muscle: correlations with body mass index and age. Mitochondr Physiol Netw 10(9):14–15. http://www.mitophysiology.org/index.php?gnaigere
43. Scheibye-Knudsen M, Quistorff B (2009) Regulation of mitochondrial respiration by inorganic phosphate; comparing permeabilized muscle fibers and isolated mitochondria prepared from type-1 and type-2 rat skeletal muscle. Eur J Appl Physiol 105:279–287
44. Aragonés J, Schneider M, Van Geyte K et al (2008) Deficiency or inhibition of oxygen sensor Phd1 induces hypoxia tolerance by reprogramming basal metabolism. Nat Genet 40:170–180
45. Kuznetsov AV, Lassnig B, Margreiter R, Gnaiger E (1998) Diffusion limitation of oxygen versus ADP in permeabilized muscle fibers. In: Larsson C, Påhlman I-L, Gustafsson L (eds) Biothermo kinetics in the post genomic era. Chalmers Reproservice, Göteborg, pp 273–276
46. Gnaiger E, Forstner H (eds) (1983) Polarographic oxygen sensors. aquatic and physiological applications. Springer, New York
47. Gnaiger E (2010) Oxygen calibration and solubility in experimental media. Mitochondr Physiol Netw 6(3):1–20. http://www.oroboros.at
48. Fasching M, Gnaiger E (2010) Instrumental background correction and accuracy of oxygen flux. Mitochondr Physiol Netw 14(6):1–12. http://www.oroboros.at
49. Kuznetsov AV, Veksler V, Gellerich FN, Saks V, Margreiter R, Kunz WS (2008) Analysis of mitochondrial function in situ in permeabilized muscle fibers, tissues and cells. Nat Protoc 3:965–976
50. Gnaiger E, Steinlechner R, Keriel C, Leverve X, Rossi A, Saks V, Sibille B, Kay L, Novel V, Daneshrad Z, Gellerich FN, Eberl T, Skladal D, Sperl W, Margreiter R (1995) Oxygen sensitivity of respiration in endothelial cells, hepatocytes and permeabilized muscle fibers studied by high-resolution respirometry. J Mol Med 73:B39